



Testing Exponential-Random Cloud Overlap for HWRF Operations and Unifying RRTMG Radiation Codes in Operational Use at NOAA/EMC

Michael J. Iacono and John M. Henderson
Atmospheric and Environmental Research
131 Hartwell Avenue, Lexington, Massachusetts 02421-3126
(E-mail: miacono@aer.com)

Final Project Report

Developmental Testbed Center (DTC) Visitor Program 2019-2020

August 2021

1. Overview

The main objectives of this project for the Developmental Testbed Center Visitor Program were to test the exponential-random (ER) cloud overlap method in HWRF (*Bernardet et al.*, 2015; *Biswas et al.*, 2018) in the RRTMG radiation code developed at AER (*Iacono et al.*, 2008) and to review and advise the DTC on the different versions of this radiation code in use at NOAA. ***Based in part on this collaborative research with the DTC, the Environmental Modeling Center (EMC) adopted the AER/RRTMG ER cloud overlap method with a constant decorrelation length in the operational HWRF for the 2020 hurricane season.*** This outcome was supported through testing of the physics change in multiple new simulations using several cloud overlap configurations that were performed by AER and by the DTC during this project. These experiments showed sufficient improvement in tropical cyclone track forecasts using the exponential-random method to justify its operational application. In addition, an examination of the RRTMG code in HWRF, which uses a version of the code released with the Weather Research and Forecasting (WRF) model, and in GFSv15, which uses a version of the code that was significantly modified by EMC, was completed to document whether the differences were stylistic, scientific, or both. The results of these activities were communicated through several presentations during the project.

Recommendations: The exponential (EXP) and ER cloud overlap methods were each tested in HWRF using two different configurations in which the specification of the required decorrelation length (DL) was either constant or spatially varying. Although the modest scale of testing and validation that was accomplished during this visitor project was not extensive enough for us to draw definitive conclusions about which overlap configuration has the most potential to improve hurricane forecast skill with HWRF, we can make the following recommendations:

- 1) The ER method should be considered a higher priority for operational use than EXP,
- 2) The distinction between the constant and latitude-varying DL may be small for TC prediction, since the two methods specify the same DL values near 20° N. However, the relative contribution of the two DL methods will increase away from this latitude,
- 3) The sensitivity of TC predictions to whether the cloud overlap and DL methods are defined consistently or differently in HWRF and in the global model used to provide boundary conditions has not been tested, though consistent settings are recommended,
- 4) This effort found only negligible scientific differences among the WRF, HWRF and GFS versions of RRTMG despite extensive coding differences related to formatting style and computational performance,
- 5) This work supports the continued use of the GFS version of the RRTMG radiation code (with appropriate upgrades when available) in future global and tropical cyclone forecast applications in the Unified Forecast System (UFS), until RRTMGP becomes available for this purpose, rather than the RRTMG code distributed in WRF.

2. Background

2.1 Cloud Overlap

The representation of the sub-grid scale properties of clouds in dynamical models remains a significant source of uncertainty in weather forecasts and climate projections. This uncertainty relates to the horizontal inhomogeneity of cloud microphysical properties and the vertical correlation or overlap of clouds and their impacts on cloud radiative processes. Understanding each of these effects is critical to simulations of the atmosphere (*Wu and Liang, 2005*). Biases associated with these processes have been shown to compensate to some degree (*Nam et al., 2012; Shonk et al., 2010b*), which reinforces the need both to study them independently and to improve them in combination.

Of importance to the project tasks is the application within RRTMG of the Monte-Carlo Independent Column Approximation (McICA; *Barker et al., 2007; Pincus et al., 2003*), which is a statistical technique for representing the sub-grid variability of clouds within the radiative transfer calculations. At present, McICA is used to represent the cloud fraction and vertical correlation of clouds. Cloud overlap assumptions in RRTMG include random (no correlation between disassociated, separated cloud layers), maximum (fully overlapping in the vertical within adjacent, multiple cloud layers), and a blend of these two called maximum-random (maximum overlap in adjacent cloud layers and random overlap among separated groups of cloud layers) first described by *Geleyn and Hollingsworth (1979)*. During our previous DTC/VP efforts, RRTMG was modified to use the exponential and exponential-random (*Hogan and Illingworth, 2000; Shonk, et al., 2010a*) cloud overlap methods, which presume that the vertical correlation within a group of adjacent cloud layers transitions inverse exponentially from maximum to random with increasing distance. The exponential (EXP) and exponential-random (ER) methods are in effect a compromise between the more extreme random and maximum-random (MR) assumptions. The EXP and ER approaches define the exponential transition, α , of cloud overlap from maximum to random within continuous cloud layers as a function of upward vertical distance through the cloud, Δz , and a decorrelation length, Z_0 :

$$\alpha = e^{-(\Delta z/Z_0)}. \quad [1]$$

High decorrelation lengths ($\alpha \rightarrow 1$) infer a greater tendency toward maximum overlap, and low decorrelation lengths ($\alpha \rightarrow 0$) infer a greater tendency toward random overlap. Finely spaced vertical layering implies smaller values of Δz , higher α , and maximum overlap, while coarser vertical spacing corresponds to higher values of Δz , lower α , and more random vertical correlation. Through multiple adjacent cloudy layers, the vertical correlation trends toward random overlap as the exponential transition is applied at each layer. The difference between EXP and ER is subtle

but potentially radiatively significant. In EXP overlap, the exponential transition and the specification of α occurs through all layers regardless of the cloud configuration. In ER overlap, the presence of at least one clear layer between cloudy layers introduces a degree of randomization in that the exponential transition within non-adjacent blocks of cloudy layers are correlated randomly, which is specified by setting α to zero within any clear layers between cloudy layers. As discussed by *Hogan and Bozzo* (2016), the EXP approach (which they refer to as EXP-EXP) generally underestimates total cloud cover relative to ER, and in some configurations EXP can even underestimate total cloud cover relative to MR overlap.

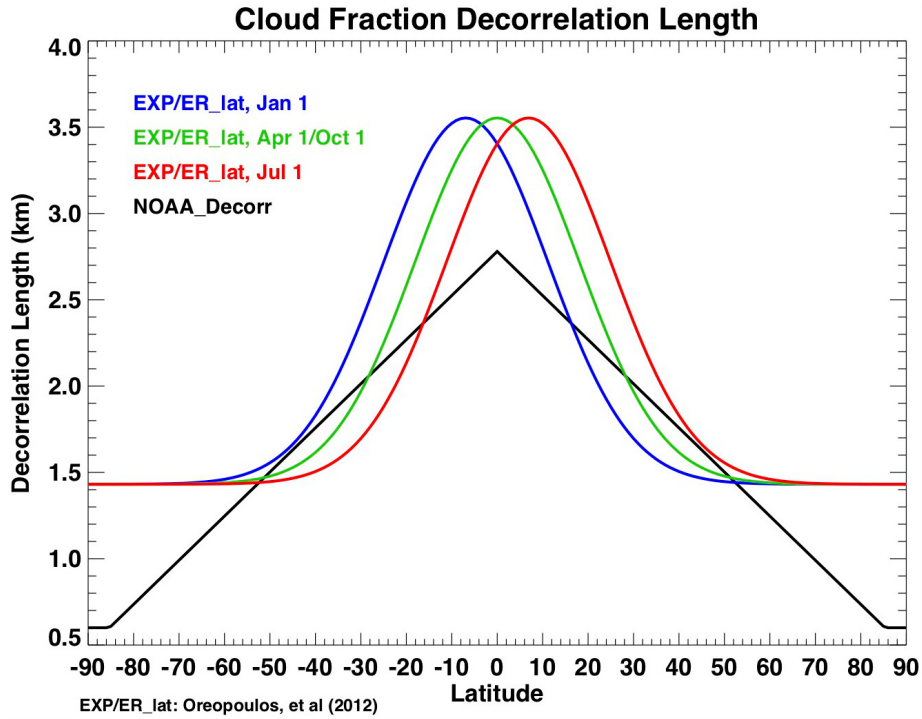


Figure 1. Decorrelation length as a function of latitude for the latitude-varying and day of year varying method of *Oreopoulos et al.*, (2012) plotted for January 1 (blue), July 1 (red), April 1 and October 1 (green). Also shown is the latitude-varying decorrelation length method of *Hogan and Bozzo* (2016) implemented by NOAA (black).

Considerable uncertainty remains regarding the optimal specification of the decorrelation length, and two methods were used during this project. Following our previous HWRF experiments, a constant decorrelation length of 2.5 km was used as a representative tropical value consistent with radar cloud measurements (*Pincus et al.*, 2005). We have also implemented a method that allows the decorrelation length to vary by latitude and by day of year (*Oreopoulos et al.*, 2012), which applies lower decorrelation length values (~1.5 km) at high latitude where cloud vertical correlation is more random and higher values (~3.5 km) at low latitude where cloud vertical correlation tends more toward maximum in deep convection. Decorrelation length values as specified by this method are illustrated in Figure 1 at three-month intervals during the year. Also shown in Figure 1 (labeled ‘NOAA_Decorr’) is the latitude-varying decorrelation length method

of *Hogan and Bozzo* (2016), which does not vary by day of year and covers a different range of DL values. The latter method was implemented by NOAA/EMC as an optional cloud overlap method for the global forecast system and is currently operational with RRTMG in GFSv16.

2.2 Microphysics

Another essential component of effectively testing the radiative impacts of vertical cloud overlap assumptions is representing the distribution of partial cloudiness in the forecast model in a realistic way, since cloud overlap is only relevant in partial cloud conditions. Dr. Greg Thompson has advanced this aspect of HWRF with a cloud fraction parameterization (ICLOUD=3 name-list option), which provides a more realistic distribution of fractional cloudiness than the previously available options in WRF. Although the Thompson-Eidhammer microphysics scheme is not currently used in the operational HWRF, Dr. Thompson has also upgraded that scheme to improve the coupling of cloud properties to the RRTMG radiation, by diagnosing the effective particle sizes of cloud water, cloud ice and snow for the radiation code. Our experiments used the default HWRF microphysics scheme (i.e., the modified tropical Ferrier-Aligo method) for the versions we applied. Our participation in the DTC Visitor Program continues to provide the opportunity to work with Dr. Thompson on evaluating and optimizing the representation of clouds and the interactions between the radiation and microphysics parameterizations in HWRF.

2.3 HWRF Configurations

During this project, two versions of HWRF were utilized, the DTC “H218” version (HWRF_v4.0a; *Biswas et al.*, 2018) and the DTC “H220” version. All code was obtained from the DTC HWRF code repository¹. TC forecasts for this project were completed by AER using H218 (from model simulations performed during our earlier efforts for DTC) and were completed by DTC on behalf of AER using H220 both to accomplish the proposed tasks and to inform the development of the 2020 operational HWRF. Within both versions we continued to use the cloud fraction parameterization developed by Dr. Greg Thompson, which was designed to provide a more realistic distribution of fractional cloudiness in HWRF. The option is activated using the ICLOUD=3 WRF name-list setting. This option is especially relevant to the forecasts performed for this project, since the cloud overlap assumption used in the radiative transfer is strongly dependent on the sub-grid cloud fraction defined by the host model. All HWRF runs used the RRTMG longwave and shortwave radiation options. The three HWRF nested grids (where the outer grid is initialized with GFS model data) were used with the standard grid spacings of 13.5, 4.5, and 1.5 km. Each of the tropical cyclones examined were forecast using multiple 126-hour forecast cycles that were initialized at 6-hour intervals. For each cycle, the parent domain was initialized from the GFS analysis. For the first (i.e., cold start) cycle of each storm, the nests were

¹ <https://svn-dtc-hwrf.ogd.ucar.edu/trunk/>

initialized from the 6-hour forecast made by the Global Data Assimilation System (GDAS). The GDAS forecast was then updated with vortex initialization and data assimilation to create the final initial condition for the nests. Warm-start cycles used a similar procedure to initialize the nests, except that the tropical cyclone vortex was obtained from the previous 6-hour HWRF forecast instead of from GDAS. This arrangement ensured that the effects of the cloud overlap modifications were carried from one forecast cycle to the next through any atmospheric state changes, but only within the tropical cyclone vortex. Our runs with H218 used the GDAS ensemble to estimate the ensemble contribution to the background error covariance to improve the efficiency of the runs while still providing a valid context for the assessment of the physics changes.

During June 2020, DTC performed eight simulations using the H220 HWRF that were designed to show the sensitivity of Joaquin's track to the choice of cloud overlap technique. The focus was on the model performance of the 00 UTC 1 October 2015 forecast cycle. At this time, Hurricane Joaquin was a major hurricane (located at 23.9 N, 72.9 W with a central pressure of 951 mb and a maximum wind speed of 100 knots) moving slowly southwest toward the Bahamas from the northeast. Four simulations (denoted "WARM") utilized the full HWRF workflow to form warm starts of each cycle from the entire history of Joaquin leading up to 00 UTC 1 October 2015, including data assimilation with available archived data and post-processing, to mimic the operational framework as closely as possible. These H220 runs differ from 2020 operational HWRF by deriving the background error covariance from the global GDAS ensemble (as used in 2015) instead of the HWRF ensemble (as done in 2020), by excluding one-way coupling to waves (not expected to impact these runs), and by using all eligible information for data assimilation (some of which may have been missed in operations). Four other simulations (denoted "COLD") were initialized from GFS and GDAS initial conditions (ICs) as a cold start at 00 UTC 1 October 2015. That is, there was no data assimilation cycling prior to the initial vortex relocation. By design, the ICs of these runs were identical, and subsequent simulation differences result from the contributions of the sub-grid scale clouds. Each of the two sets of four simulations comprise the four combinations of the EXP (option 4) and ER (option 5) cloud overlap techniques and the fixed decorrelation length method (option 0; using a value of 2500 m) or the latitudinally and seasonally varying decorrelation length method (option 1).

In September 2020, a small discrepancy was discovered in the processing of the specific humidity lateral boundary condition (BC) related to a dependence on the version of the NOAA computer system "jet" that was used to create the specific humidity field. To avoid the complication introduced by this discrepancy on interpreting the final TC forecast results, all eight of the Joaquin H220 simulations were repeated by DTC using consistent lateral BCs. This latter set of runs, which were notably different from the initial set, are analyzed here.

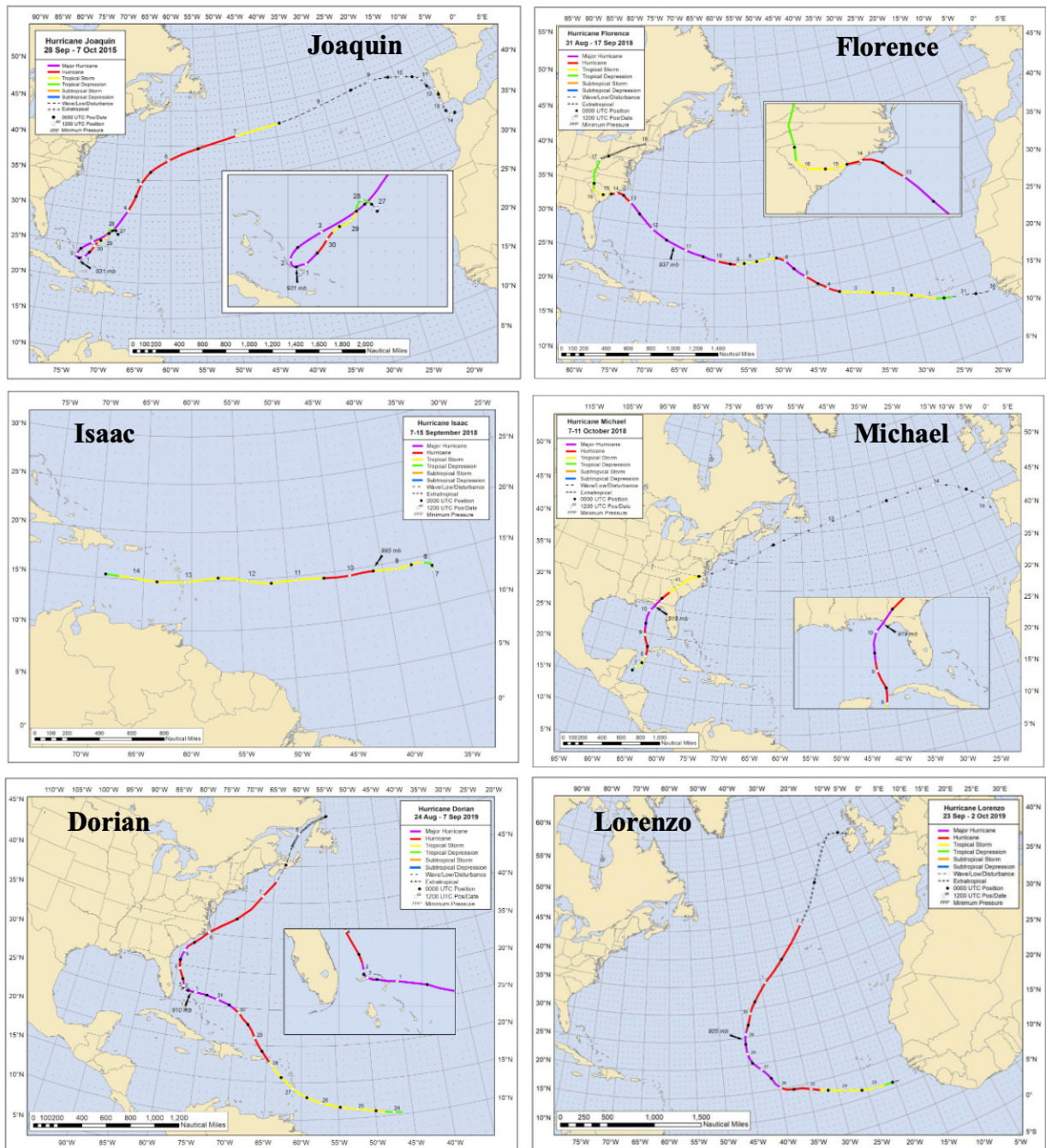


Figure 2. Best track paths of Hurricane Joaquin through the northwest Atlantic from 28 September to 7 October 2015 (top left), Hurricane Florence across the Atlantic basin from 30 August to 15 September 2018 (top right), Hurricane Isaac across the central Atlantic from 7 to 15 September 2018 (center left), Hurricane Michael from the western Caribbean through U.S. landfall from 7 to 11 October 2018 (center right), Hurricane Dorian through the western Atlantic basin from 24 August to 7 September 2019 (bottom left), and Hurricane Lorenzo across the central Atlantic basin from 23 September to 2 October 2019 (bottom right). Best track graphics provided by the NOAA National Hurricane Center.

2.4 Tropical Cyclone Cases

This project assessed the effects of the cloud overlap change on the evolution of several recent, high-impact tropical cyclone cases including hurricanes Joaquin, Florence, Isaac, Michael, Dorian, and Lorenzo. Hurricane Joaquin was an Atlantic (ATL) basin TC that was active from 25 September to 8 October 2015 (*Berg, 2016*). This storm reached Category 4 intensity and followed a highly unusual track through the northwestern Atlantic, shown in Figure 2 (top left panel), which remained a forecasting challenge for many of the operational, hurricane forecast models through much of the storm’s lifetime. This TC was examined for this project because of the high sensitivity of its track and intensity to the cloud overlap method that was documented in our earlier DTC research (*Iacono and Henderson, 2019*). Hurricane Florence was another Cape Verde Atlantic basin TC that left the coast of Africa on 30 August 2018 and made landfall in North Carolina on 14 September 2018. This storm rapidly intensified from a tropical storm to a Category 4 hurricane in about 36 hours from 9-10 September 2018. Although it weakened to Category 1 by landfall, it was a high impact storm that caused catastrophic flooding over North and South Carolina. Hurricane Isaac was active over the central Atlantic from 7 to 15 September 2018 and became a minimal hurricane for one day before weakening as it approached the Windward Islands. Hurricane Michael was active from 7 to 11 October 2018 and was one of the few storms to reach Category 5 intensity that made landfall in the United States (*Beven et al., 2019*). This hurricane experienced rapid intensification while moving northward through the eastern Gulf of Mexico and made landfall near Mexico Beach, Florida with maximum sustained winds estimated to be near 160 mph. Hurricane Dorian was a very high impact tropical cyclone and one of the strongest ever to form over the western Atlantic. It was active from 24 August to 7 September 2019 and caused catastrophic damage to the northern Bahamas over several days as a Category 5 storm with maximum sustained winds of 180 mph or more. Slower movement and a sharp turn to the north

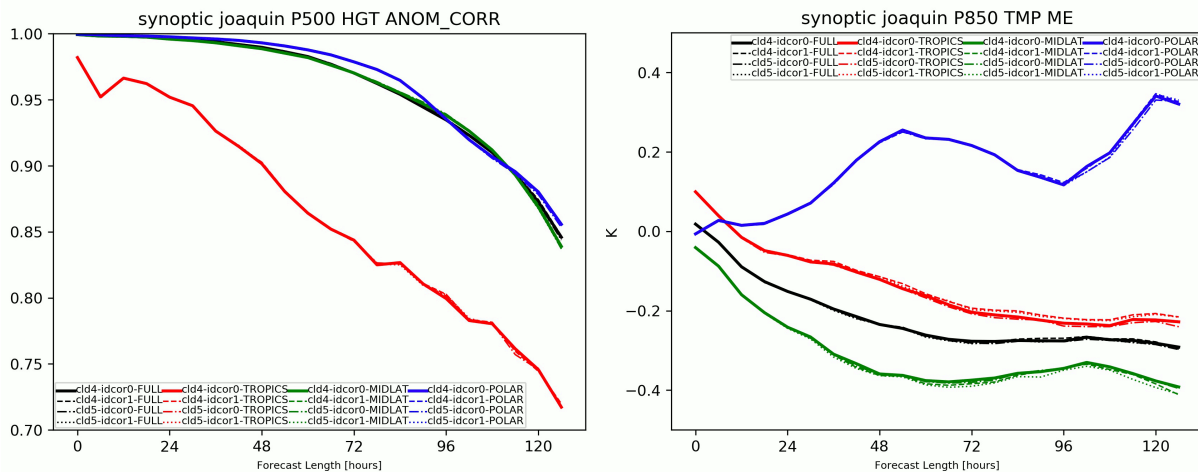


Figure 3. Hurricane Joaquin anomaly correlation of 500 hPa height (left) and mean error of 850 hPa temperature (right) averaged over 36 forecast cycles from 06 UTC on 29 September 2015 to 00 UTC on 8 October 2015 as simulated by H218 over the “synoptic” grid shown for the full grid (black), tropical (red), mid-latitude (green), and polar (blue) latitudes and for four different combinations of vertical cloud overlap and decorrelation length.

along the southeastern U.S. coast narrowly prevented significant damage to the coast of Florida. Finally, Hurricane Lorenzo was active over the central to northern Atlantic from 23 September to 2 October 2019. After moving westward initially, Lorenzo moved northward through a break in the subtropical ridge. It experienced two periods of rapid intensification reaching Category 5 intensity during the second period on 29 September well west of the Azores before weakening very rapidly and dissipating over the north Atlantic.

3. Results and Discussion

3.1 H218 Testing: Hurricane Joaquin Anomaly Correlation and Mean Errors

Using HWRP predictions of Hurricane Joaquin completed using H218 during our previous DTC efforts, we examined the anomaly correlation and mean error of several parameters to assess the impact of modifying the cloud overlap and decorrelation length options. Anomaly correlations and mean errors were examined over the H218 “synoptic” grid as simple averages over thirty-six 126-hour forecast cycles initialized at six-hour intervals covering much of the life cycle of Joaquin from 06 UTC on 29 September 2015 to 00 UTC on 8 October 2015. Figure 3 shows the anomaly correlation (AC) for 500 hPa geopotential height (left panel) and the mean error (ME) of 850 hPa temperature (right panel) at 3-hour intervals over the average forecast cycle. The AC and ME are shown for the entire d01 grid (in black), and for tropical (20° S to 20° N, in red), mid-latitude (20° – 60° N, in green) and polar (poleward of 60° N, in blue) latitude bands within the d01 grid. In addition, the AC and ME are shown for four different combinations of vertical cloud overlap and decorrelation length (Z_0) method including EXP (“cld4”) with constant Z_0 (solid line), EXP with spatially varying Z_0 (dashed line), ER (“cld5”) with constant Z_0 (dashed-dotted line), and ER with spatially varying Z_0 (dotted line). Only negligible differences are noted among the 500 hPa AC plots, while differences in 850 hPa temperature mean error are noticeable, especially in the tropical and mid-latitude regions.

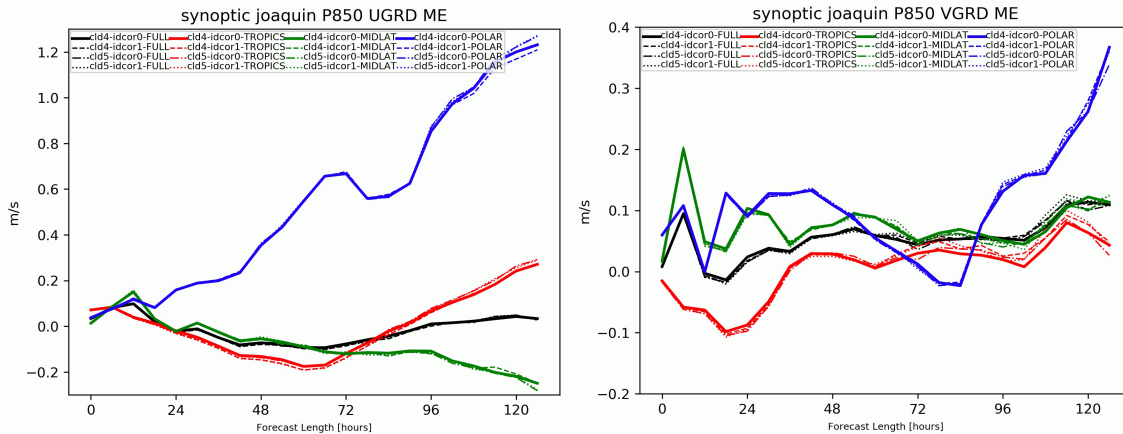


Figure 4. Hurricane Joaquin mean errors of 850 hPa zonal wind speed (left) and 850 hPa meridional wind speed (right) averaged over 36 forecast cycles from 06 UTC on 29 September 2015 to 00 UTC on 8 October 2015 as simulated by H218 over the “synoptic” grid shown for the full grid (black), tropical (red), mid-latitude (green), and polar (blue) latitudes and for four different combinations of vertical cloud overlap and decorrelation length.

Mean errors of 850 hPa zonal wind speed (left panel) and 850 hPa meridional wind speed (right panel) are shown in Figure 4 at 6-hour intervals over the average forecast cycle. The ME are shown for the same spatial areas and cloud overlap combinations as in Figure 3. In these experiments, the zonal wind ME is largest for the polar region, where the cloud overlap methods have a small impact on average during the last day of the forecast cycle. Small zonal wind ME differences are seen in the tropical and mid-latitude regions. Mean errors in meridional wind speeds are generally smaller and are most noticeable in the tropical and mid-latitude regions.

3.2 H220 Testing: DTC and EMC Tropical Cyclone Test Cases

In consultation with EMC, the DTC performed pre-implementation testing during early 2020 with a small set of tropical cyclones using the preliminary version of the H220 model. These tests were completed in support of this project and to inform the decision of which cloud overlap method to apply in the 2020 operational HWRF. The original set of TC cases examined in these tests included Hurricanes Florence, Isaac, Dorian, and Lorenzo. The full life cycle of each TC was predicted with a sequence of 126-hour forecast cycles using two different cloud overlap configurations: 1) exponential overlap with constant decorrelation length of 2500 m (H20C), and 2) exponential-random overlap with latitude-varying decorrelation length (H20R). An initial assessment of the track and intensity error statistics from these runs over the full sample of storms showed only small overlap related impacts on track and intensity. Since the constant decorrelation length used in H20C is very similar to the latitude-varying decorrelation length used in H20R over the 20-25° N latitude band (see Figure 1), the track and intensity error statistics were re-examined for both the full sample and a latitude-restricted sample. Figure 5 shows the track error for the set of four TCs listed above averaged over the full sample (left panel) and over the latitude range 17.5-27.5° N (right panel), which was chosen to retain an adequate sample size. The expectation is that the full sample track error will reflect differences in both cloud overlap and decorrelation length method and that the restricted spatial sample will more closely (though not rigorously) reflect differences only in the cloud overlap method. Figure 5 shows that ER provides noticeable improvement in track error over EXP for the latitude restricted TC sampling.

As a next step, DTC and EMC made two additions to the testing configuration. At our request, two TC cases were added, Hurricane Michael, and Hurricane Leslie, which was a long-lived TC in the eastern Atlantic during 2018 that initially followed a very meandering track before heading eastward and making landfall in Portugal as an extratropical storm. It was also decided to rerun the original set of four TC cases and the two additional storms using ER cloud overlap with a constant decorrelation length of 2500 m (H2R1) to assess more rigorously the impact of the cloud overlap change (relative to H20C) in isolation from the decorrelation length method. A large set of evaluation statistics were prepared to assess the impact of these experiments.

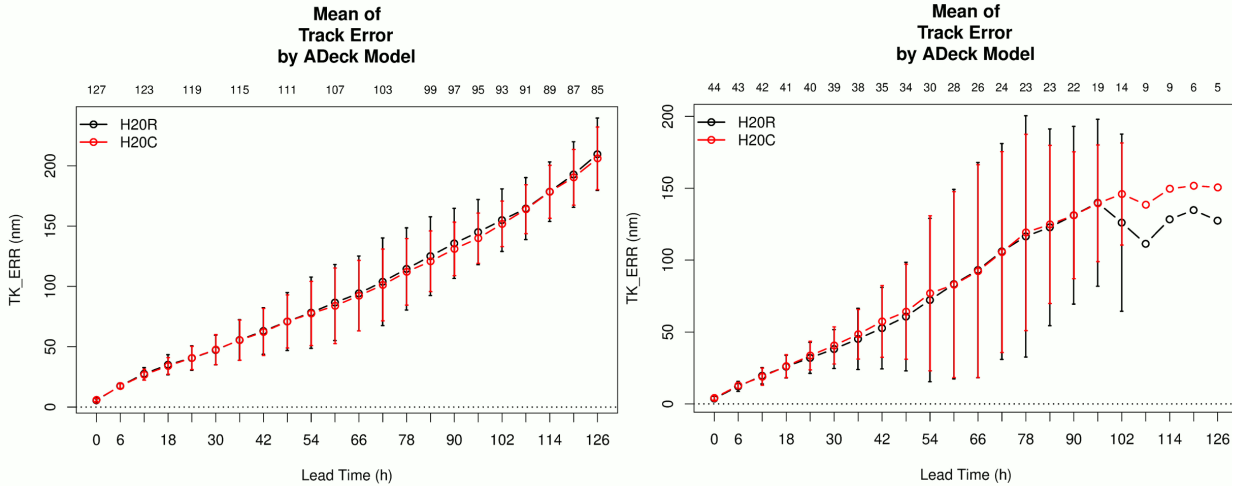


Figure 5. Mean track error as a function of forecast time for H220 running a small sample of hurricanes (Florence, Isaac, Dorian, and Lorenzo) for two cloud overlap methods, EXP with constant decorrelation length (H20C) and ER with latitude-varying decorrelation length (H20R) averaged over the full sample (left panel) and over the latitude range 17.5-27.5° N. Graphics provided by Evan Kalina (CIRES at NOAA/GSL, DTC). The number of simulations represented at each forecast time is indicated above the top axis in each panel.

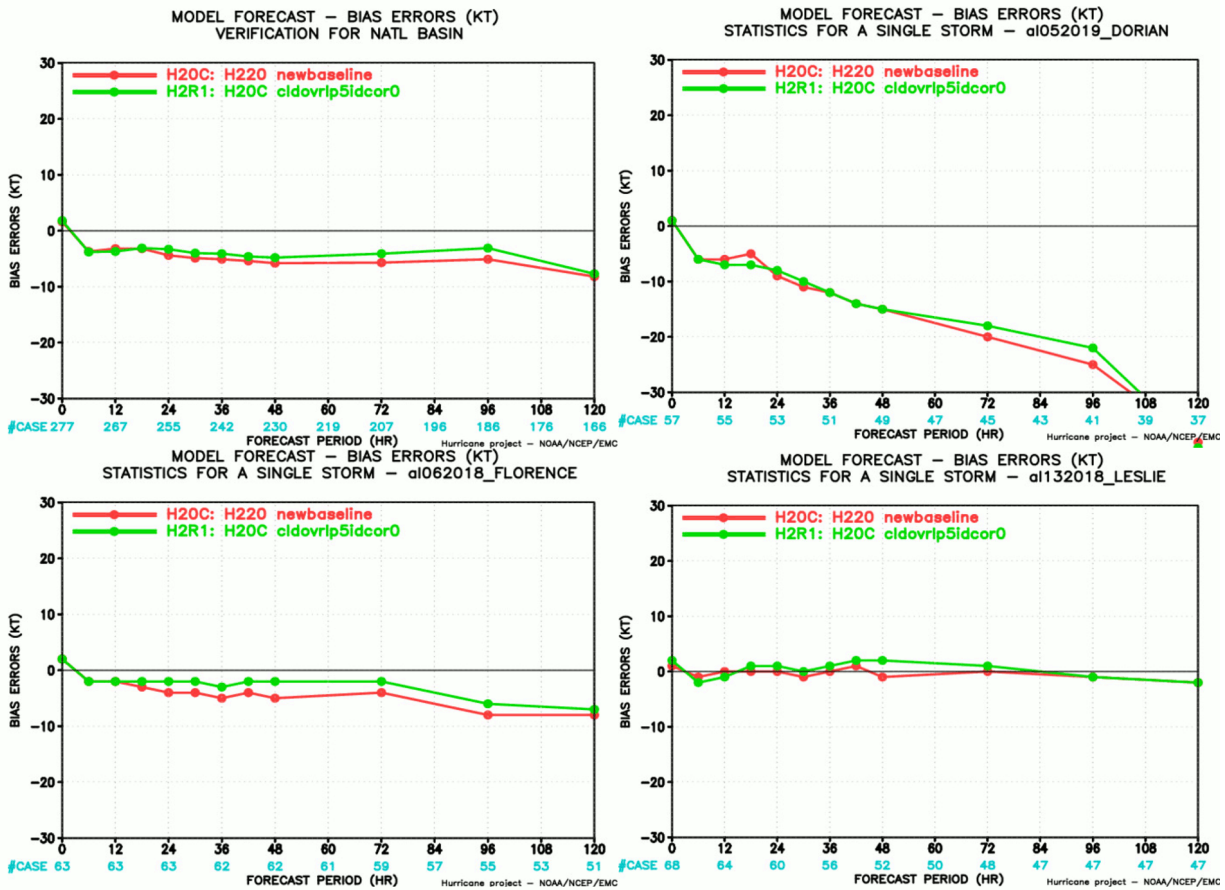


Figure 6. H220 predicted bias errors (in knots) for two sets of tropical cyclone predictions using EXP cloud overlap (H20C; red) and ER cloud overlap (H220R1; green) for an average over six North Atlantic TCs (top left) and for Hurricanes Dorian (top right), Florence (bottom left) and Leslie (bottom right). Graphics provided by Bin Liu (IMSG at NOAA/EMC).

H220 predicted wind speed bias errors for the two cloud overlap methods are shown in Figure 6 for all six TC cases over the full Atlantic basin (top left) and for individual storms Dorian (top right), Florence (bottom left) and Leslie (bottom right). In these tests, ER produces smaller bias errors relative to EXP for the basin average and for Florence, while similar bias errors are seen for Dorian and slightly degraded bias errors for ER are seen for Leslie. H220 predicted track errors for the two cloud overlap methods are shown in Figure 7 for all six TC cases over the full Atlantic basin (top left) and for individual storms Florence (top right), Isaac (bottom left) and Michael (bottom right). In these tests, ER slightly degrades track errors relative to EXP for the basin average and for Isaac, while improved track errors are seen for Florence and slightly improved over much of the forecast period for Michael.

Additional H220 predicted evaluation statistics for the two cloud overlap methods for all six TC cases over the full Atlantic basin are shown in Figure 8. Included in Figure 8 are along track bias in nautical miles (top left), minimum central pressure bias in hPa (top right), average

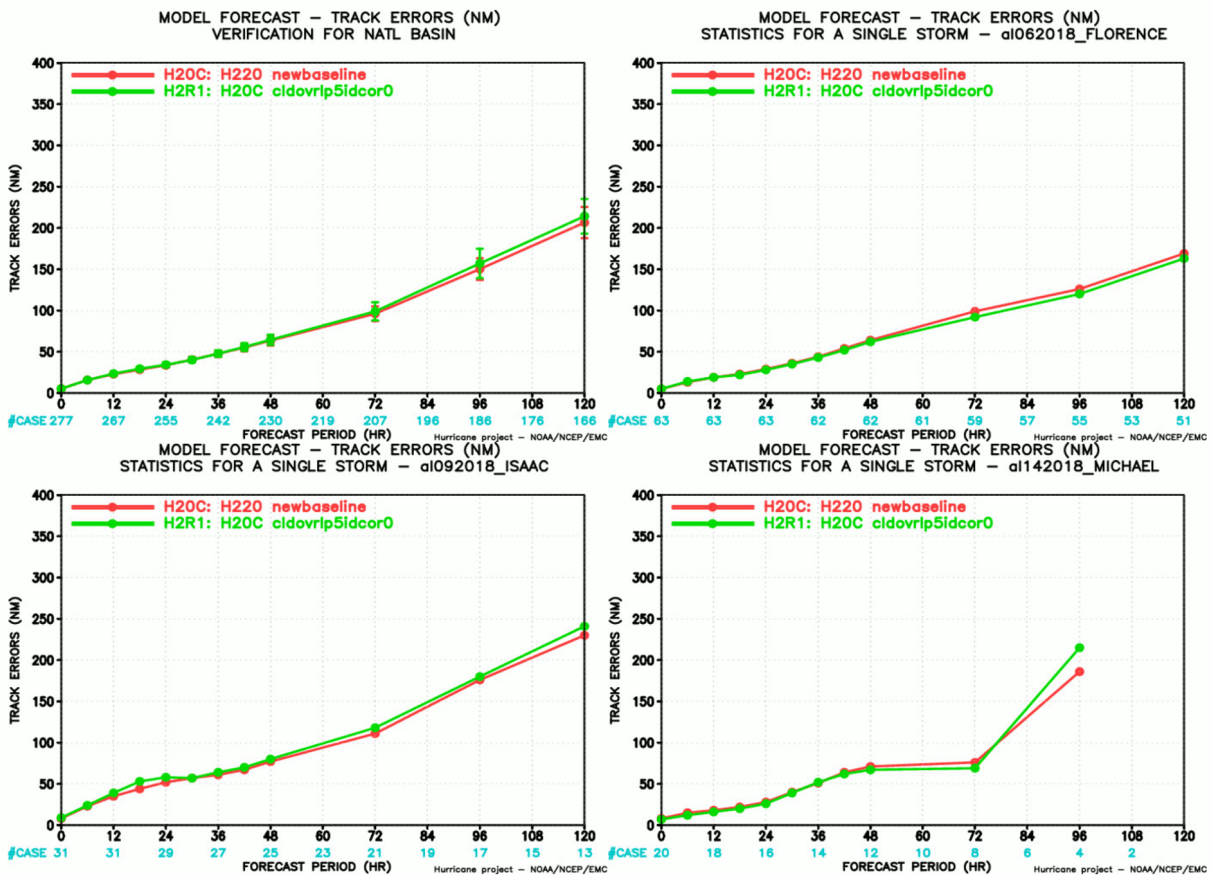


Figure 7. H220 predicted track errors (in nautical miles) for two sets of tropical cyclone predictions using EXP cloud overlap (H20C; red) and ER cloud overlap (H2R1; green) for an average over six North Atlantic TCs (top left) and for Hurricanes Florence (top right), Isaac (bottom left) and Michael (bottom right). Graphics provided by Bin Liu (IMSG at NOAA/EMC).

34-knot radius errors in nautical miles (bottom left) and average 64-knot radius errors in nautical miles (bottom right). In these statistics, ER produces neutral to slightly improved results at longer lead times relative to EXP for the TC along track bias, the central pressure bias, and the 34-knot radius errors, while neutral to slightly degraded results are seen for the 64-knot radius errors.

3.3 H220 Testing: AER Joaquin Synoptic Analysis

3.3.1 Design of Cloud Overlap Sensitivity Experiments

In support of this project, DTC performed a total of eight new H220 simulations during September 2020 that were designed to show the sensitivity of Hurricane Joaquin’s evolution to the choice of cloud overlap method. For these tests, the focus was on the model performance of the forecast cycle that was initialized on 0000 UTC 1 October 2015. At the time, Hurricane Joaquin was a major hurricane (23.9 N, 72.9 W; 951 hPa; 100 knots) moving slowly toward the Bahamas from the northeast. By design, the ICs of these runs are identical and subsequent differences result

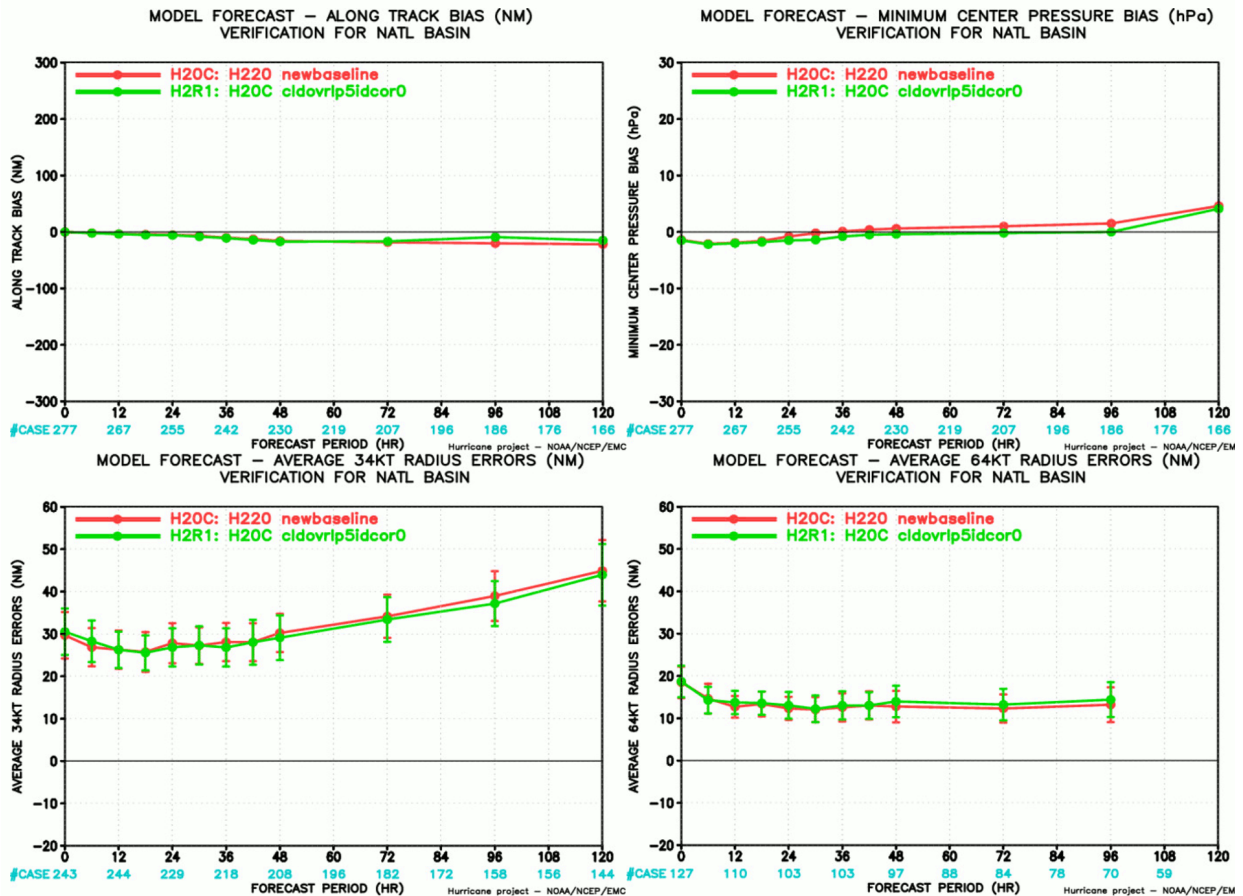


Figure 8. H220 predicted evaluation statistics for two sets of tropical cyclone predictions using EXP cloud overlap (H20C; red) and ER cloud overlap (H2R1; green) over the full set of TC Atlantic basin cases for along-track bias (top left), minimum central pressure bias (top right), average 34-knot radius error (bottom left) and average 64-knot radius error (bottom right). Graphics provided by Bin Liu (IMSG at NOAA/EMC).

from the handling of sub-grid scale clouds. Each of the two sets of four simulations comprise a matrix of four combinations of the EXP (option 4) and ER (option 5) cloud overlap approaches and constant (option 0) or latitudinally and seasonally varying (option 1) decorrelation lengths. Further details of these experiments were provided in Section 2.3.

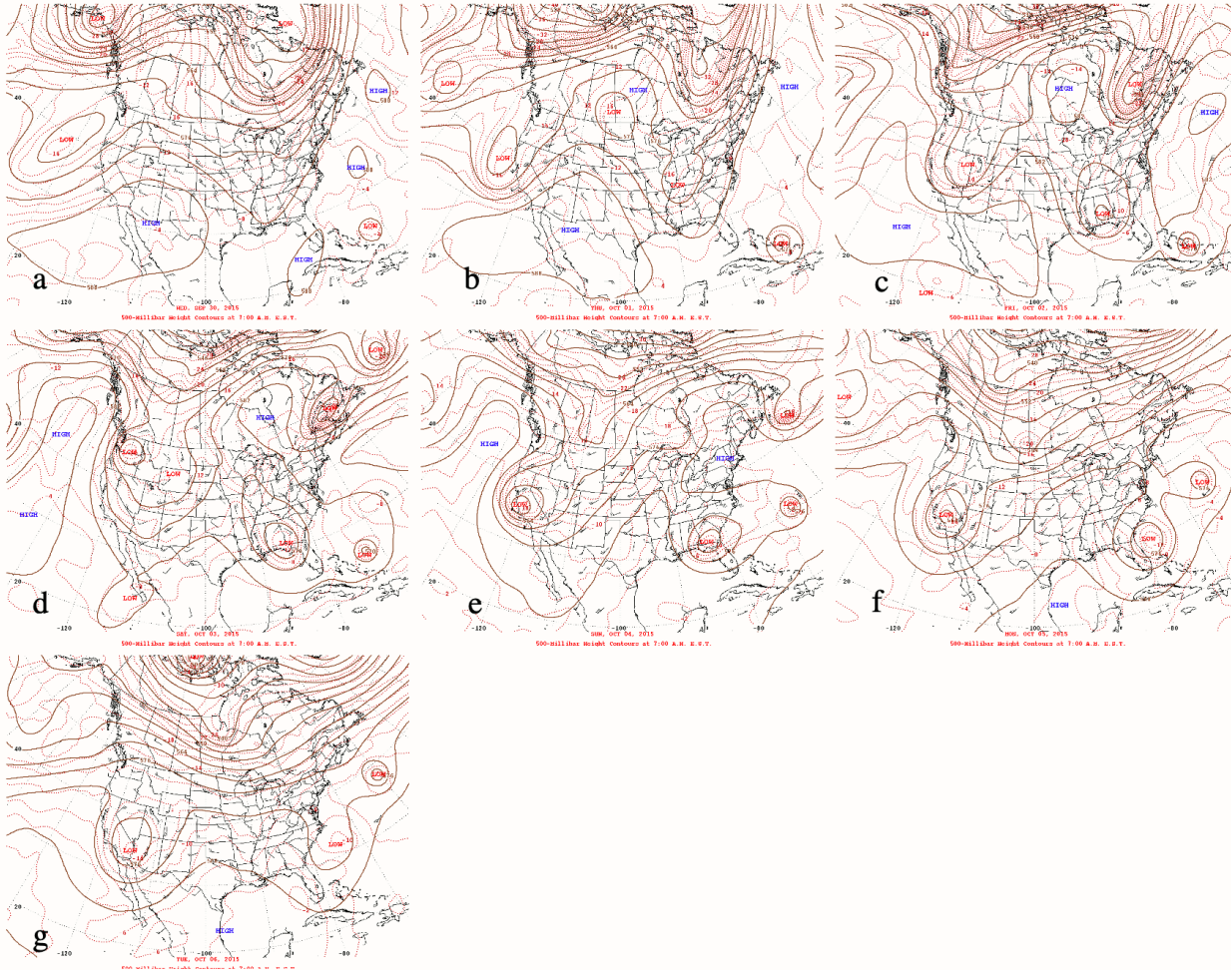


Figure 9. NCEP analyses at 12 UTC on 30 September to 2 October 2015 (top row), 3-5 October 2015 (center row), and 6 October 2015 (bottom row) showing the evolution of the 500 hPa synoptic features that affected the movement of Hurricane Joaquin.

3.3.2 Overview of the Synoptic Influences on Hurricane Joaquin

The operational, forecasted position of Hurricane Joaquin in 2015 lacked run-to-run consistency with considerable spread among different HWRF configurations and other operational models available at the time. We review the complex steering flow that affected the motion of Joaquin and, in subsequent sections, document the sensitivity of model performance to the choice of cycling and cloud overlap technique. Analysis of storm-scale physical processes is hindered by the need to examine subtle contributions to the steering flow without the ability to remove the circulation of the storm.

The NCEP Weather Prediction Center synoptic charts at 500 hPa for 30 September to 6 October 2015, shown in Figure 9, illustrate the complex synoptic-scale influences on the non-climatological motion of Hurricane Joaquin toward the southwest and its subsequent sharp turn to the northeast, which caused operational forecasts to exhibit large position errors. At 1200 UTC 30 September 2015, Hurricane Joaquin was undergoing rapid intensification while positioned northeast of the Bahamas, represented in Figure 9a as a closed low at 500 hPa. A weak ridge with several centers of high pressure separated Joaquin from a positively tilted trough over the Ohio River valley and an upstream short-wave trough over Iowa. The most prominent feature at the surface (not shown) is a cold front, associated with the upper-level trough, that extends from New England to Texas. Twenty-four hours later at 1200 UTC 1 October (Figure 9b), the 500 hPa trough is undergoing continued deepening, with a cut-off low centered over Western Kentucky. Joaquin has moved farther southwest and is positioned over the Southern Bahamas. The northern part of the surface cold front has stalled from offshore of the Georgia coast to the Canadian Maritimes. By 1200 UTC 2 October (Figure 9c), the ridge positioned to the northwest of Joaquin contributes a deep-layer northeasterly steering flow that results in the continued southwest motion of Joaquin. However, during the subsequent 96 hours (Figure 9 d-g), the ridge retreats to the northeast and Joaquin is subjected to southwesterly steering flow ahead of the upstream closed low that is positioned over the southeastern US. Historic rainfall occurred over the next few days in South Carolina as deep-layer, moisture-laden onshore flow rode over the surface front while in the presence of upper-level divergence from the upstream upper-low. During this period, Joaquin moved steadily to the northeast well offshore.

The cause of the non-climatological track taken by Hurricane Joaquin under complex steering flow (see Figure 2) has been the focus of several recent studies (e.g., *Papin et al*, 2016; *Marciano and Lackmann*, 2017; *Miller and Zhang*, 2019). The forecasted positions of Joaquin in operational model runs and subsequent research studies of Joaquin (including this one) have exhibited extreme sensitivity and lacked cycle-to-cycle consistency. Forecast spread at 5-7 days varied widely from landfall in the Carolinas – a consequence of a sharp leftward bend in the track (like the unusual track of Hurricane Sandy), which also appeared in some H218 HWRF simulations to a track well offshore, which was substantially closer to the observed track.

3.3.3 Effect of Cloud Overlap and Cycling on Joaquin Track and Intensity

The eight H220 forecast tracks for Joaquin shown in Figure 10 provide reasonable forecast guidance relative to the observed track over the 126-h forecast period, and all show the observed transition from northeasterly steering flow associated with a ridge to the north of the TC to prolonged southwesterly flow from a mid-latitude trough approaching from the west. This is a

notable improvement over many prior-year simulations. Two aspects of the tracks differentiate the cold start experiments (labelled “fC40”, “fC41”, “fC50”, and “fC51”) from the warm start experiments (labelled “fW40”, “fW41”, “fW50”, and “fW51”) that are more clearly illustrated in the close-up images of the sharp turn to the northeast seen in the first few days of this forecast cycle shown in Figure 11a for the cold start cases and in Figure 11b for the warm start cases. First, the initial motion in the warm start tracks is to the southwest, compared to a westward track in the cold start runs. As a result, Joaquin tracks farther to the south and west at short forecast ranges in the warm start cases in somewhat better agreement with the observed storm track. This suggests that the northeasterly steering flow from the upper ridge was stronger and better represented in the ICs for the warm start runs. During the first 24-48 hours, Joaquin is positioned 50-100 km farther southwest in the warm start runs, which initially delays the subsequent northward movement. However, at later forecast times around 48 hours, the eight warm and cold tracks are similar in position near 25.5 N, with the cold tracks positioned approximately 50 km farther to the west. Second, there is general agreement that the four warm start tracks verify closer to the observed storm toward the end of the forecast period with a larger meridional component of motion to the north-northeast movement of Joaquin compared to the farther east cluster of cold start simulations. The four warm start tracks feature an appreciable bifurcation to the left (north) from the tight cluster of all eight tracks at, for instance, 72 hours. It is expected that the warm start tracks benefit from the multiple cycles of data assimilation that modify the near-storm steering flow, though the storm itself is repositioned (close) to the best track position and intensity at the start of every cycle.

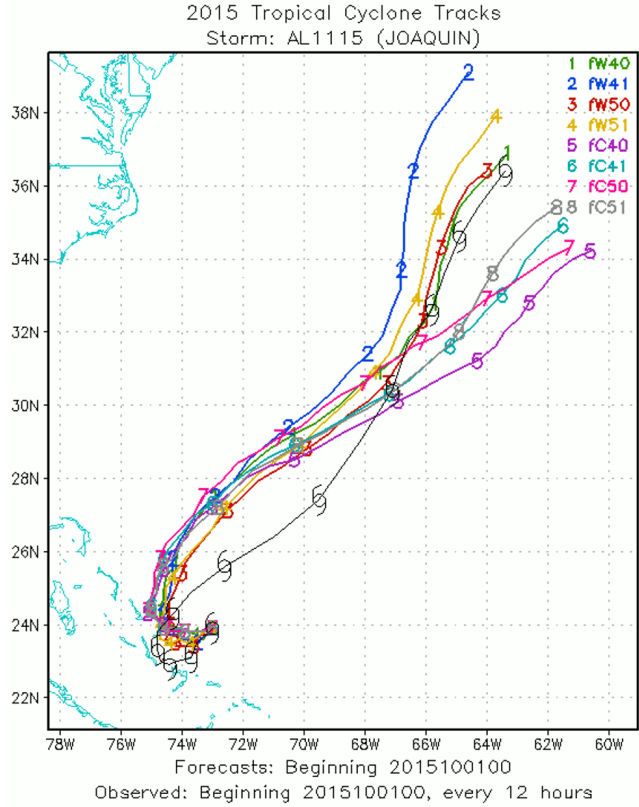


Figure 10. H220 forecast tracks with storm positions plotted every 12 hours for eight Hurricane Joaquin predictions initialized at 00 UTC on 1 October 2015 for a set of four cloud overlap configurations and using both cold start “fC” and warm start “fW” initial conditions.

The Joaquin intensity predictions were affected considerably by the application of cycling in the forecasts. Figure 12 shows that the warm start forecasts (top panel) simulated the observed low central pressure of Joaquin much better (with one exception) than did the cold starts (bottom

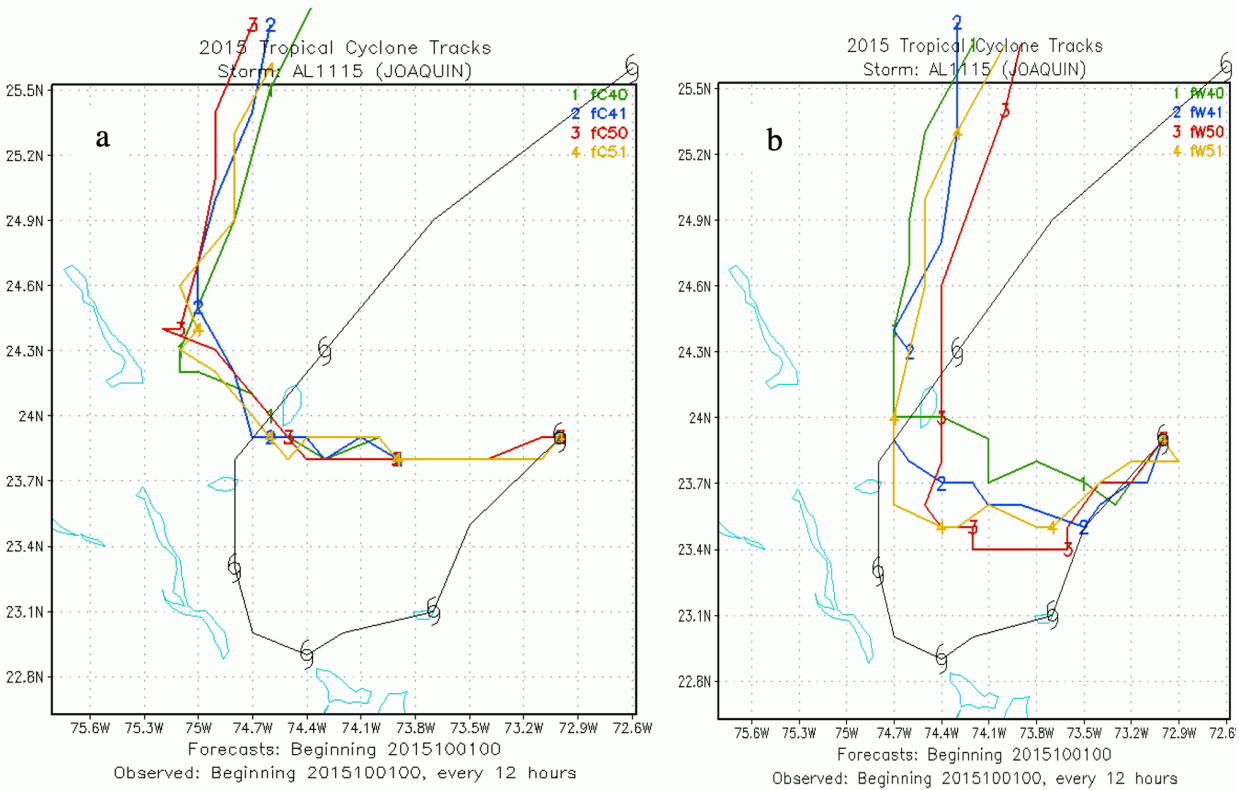


Figure 11. H220 forecast tracks with storm positions plotted every 12 hours for eight Hurricane Joaquin predictions initialized at 00 UTC on 1 October 2015 during the first 60 forecast hours for a set of four cloud overlap configurations and using both cold start (left panel) and warm start (right panel) initial conditions.

panel), despite all forecasts being initialized around 950 hPa. The warm start simulations also maintained the initial intensity more closely matching the observed intensity, while the four cold start simulations substantially weaken Joaquin by 24 hours and remain generally 20-30 hPa too weak through 72 hours and 15-20 hPa too weak through the end of the 126-hour forecast cycle. The warm start cycling may have contributed to improving the dynamical balance of the environmental fields within the vortex in the warm start ICs. In addition, the presence of a shallower storm in some simulations would likely result in an environmental steering flow that is similarly shallower than in a more robust storm with appreciable impacts on storm motion. Weaker storms may receive less influence from high altitudes (above 400 hPa), which may have played a role for Joaquin. Indeed, around 72 to 84 hours as the warm tracks began to bifurcate, these runs were about 20 hPa deeper than their cold counterparts. It should be noted that the EXP cloud overlap with fixed decorrelation length warm start simulation (labelled “fw40” in Figure 12a) exhibited characteristics like the four cold start simulations with a sea-level pressure (SLP) at times 25 hPa higher than the other warm start runs. This may have been partially in response to its initialized central pressure, which was approximately 6 hPa higher than the other warm start runs. Interaction with land is a potential source of the temporary weakening in the warm cases around 24 hours.

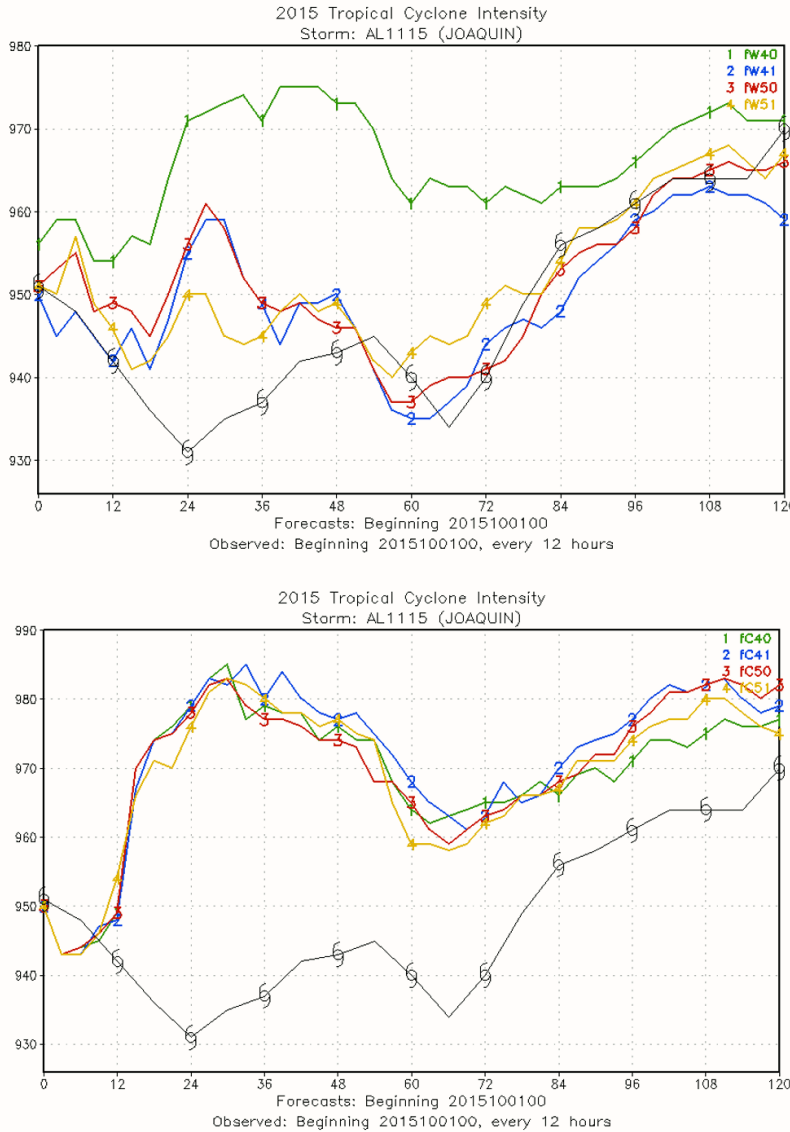


Figure 12. H220 forecast central pressure intensity of eight Hurricane Joaquin predictions initialized at 00 UTC on 1 October 2015 for a set of four cloud overlap configurations and using both warm start (top panel) and cold start (bottom panel) initial conditions.

scope of this work. Model output is available every three hours, and the cloud overlap treatments begin to exert appreciable influence on model fields well before this initial history file output time. It will be seen that the cloud overlap methods are important throughout the model domain for grid cells with partial clouds. By focusing solely on the cold start runs, we remove the influence of data assimilation cycling; differences between simulations in the initial time fields at hour 00 (not shown) are zero.

3.3.4 Effects of Cloud Overlap on Cold Start Experiments

We now analyze the performance of the four cold start simulations from 00 UTC 1 October 2015 to document differences that arise solely due to the choice of cloud overlap. For reference and for clarity, only the cold tracks from Figure 10 are reproduced in Figure 13. The primary purpose of the following time series analysis is to provide an initial evaluation of the choice of cloud overlap approach by showing simple difference fields between the various simulations. Panel-by-panel analysis is not provided. Only a rudimentary interpretation of the complex interactions of Hurricane Joaquin with the environmental flow was accomplished here; a full evaluation of the sources of model error that affect TC track differences is beyond the

Overall, the tracks are similar with the initial westward movement in all cases that is followed by recurvature to the northeast at a faster forward motion. There is small spread through 60 hours and the clustering of tracks and relatively uniform northeastward movement suggests that Joaquin at 60 hours is embedded in a robust (spatially expansive, persistent, and moderate in intensity) southwesterly flow. The model steering flow is likely not influenced by as deep a steering flow as observed, due to the weak bias in predicted SLP and wind speeds. Despite the apparent uniform flow, the tracks begin to show increased spread starting around 72 h as the environmental steering flow is modified by nearby synoptic features, with a slight increase in meridional motion in all tracks except fc50 (ER with static decorrelation). Overall, the 120-hour storm positions are closely clustered approximately 2-3 degrees to the southeast of the observed position.

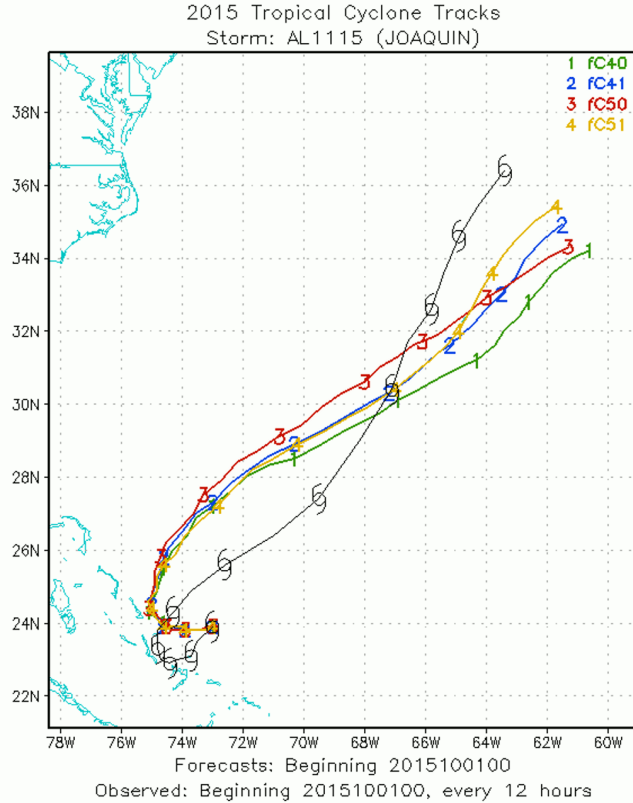


Figure 13. H220 forecast tracks of four Hurricane Joaquin predictions initialized at 00 UTC on 1 October 2015 for a set of four cloud overlap configurations using cold start initial conditions.

The statistics we present next were generated using version 8.0 of the Model Evaluation Tools (MET), maintained and distributed by DTC, applied to merged d01, d02 and d03 H220 grb2 files for the three model domains (sample filename: “joaquin11.2015100100.hwrf_sat.global.0p25.f000.grb2”). These files are on a global 0.25-degree grid, but with physical values only for regions covered by the HWRF triply nested domains. Output files were available every six hours; selected times are presented below. The model field maps were generated using “series_analysis” via a script written by John Henderson that was provided to DTC during one of our earlier DTC Visitor Program projects (available on-line at https://www.dtcenter.org/sites/default/files/community-code/hwrf/developers/codes/series_analysis.tar.gz). The statistics presented in the mean error (ME) and anomaly correlation (ANOM_CORR) line plots were generated using “grid_stat” and MetPlus. The following series of maps below show the differences over the model integration period (to 120 hours) between combinations of the cold start simulations for temperature (TMP) at 850 and 300 hPa, geopotential height (HGT) at 500 hPa, relative humidity (RH) at 850 hPa and

wind speed (WIND) at 300 hPa. Note the change in the contour color scale between the earlier and later forecast hours that allows for the time evolution of the fields to be illustrated and examined in greater detail.

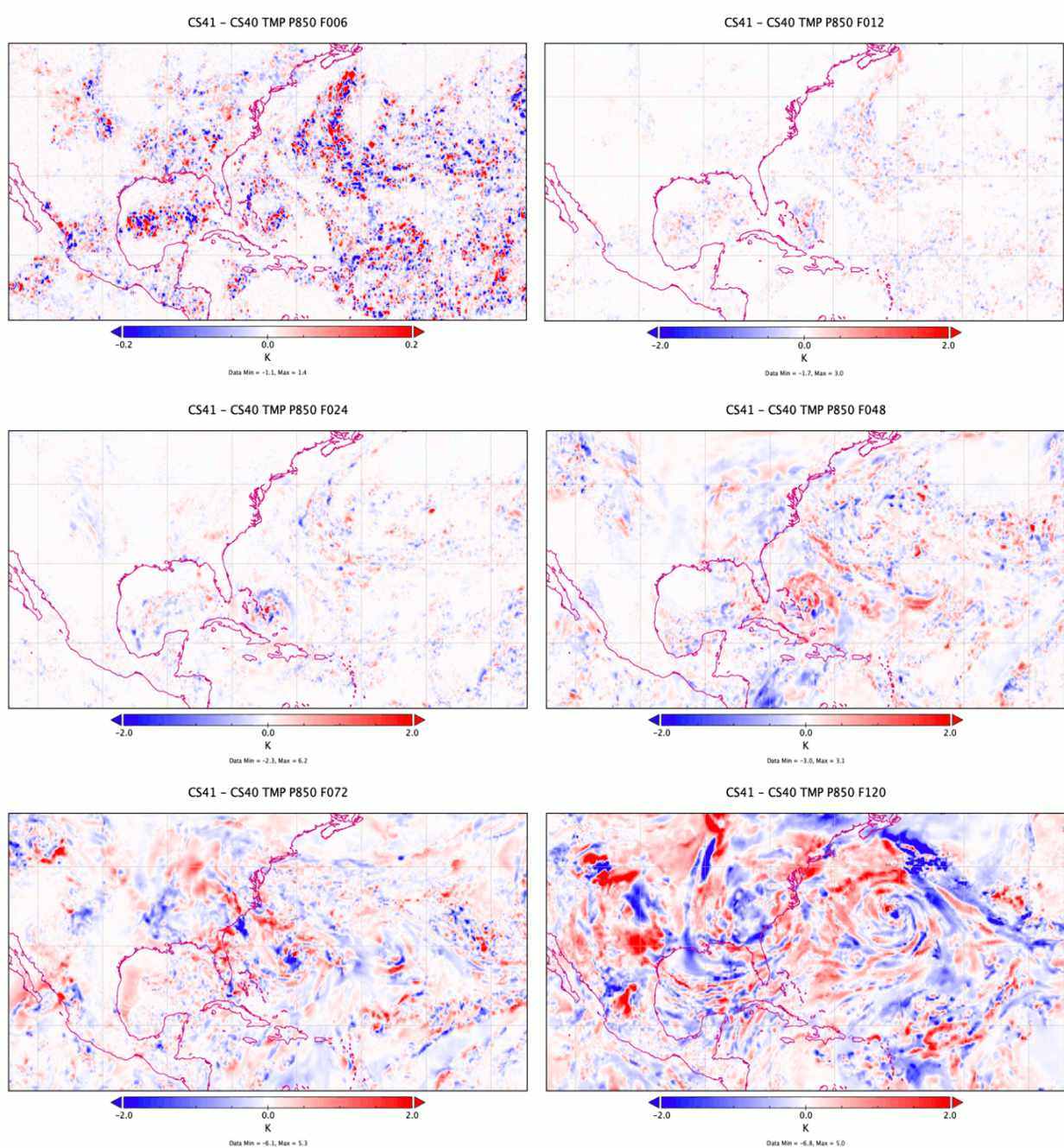


Figure 14. MET-generated differences in H220 predicted 850 hPa temperature (in K) for a forecast cycle initialized at 00 UTC 1 October 2015 of Hurricane Joaquin between model runs using EXP cloud overlap with varying decorrelation length “CS41” and EXP cloud overlap with constant decorrelation length “CS40” at six forecast times. Note the change in the color scale between the plot at 6-hours (top left) and the later forecast times.

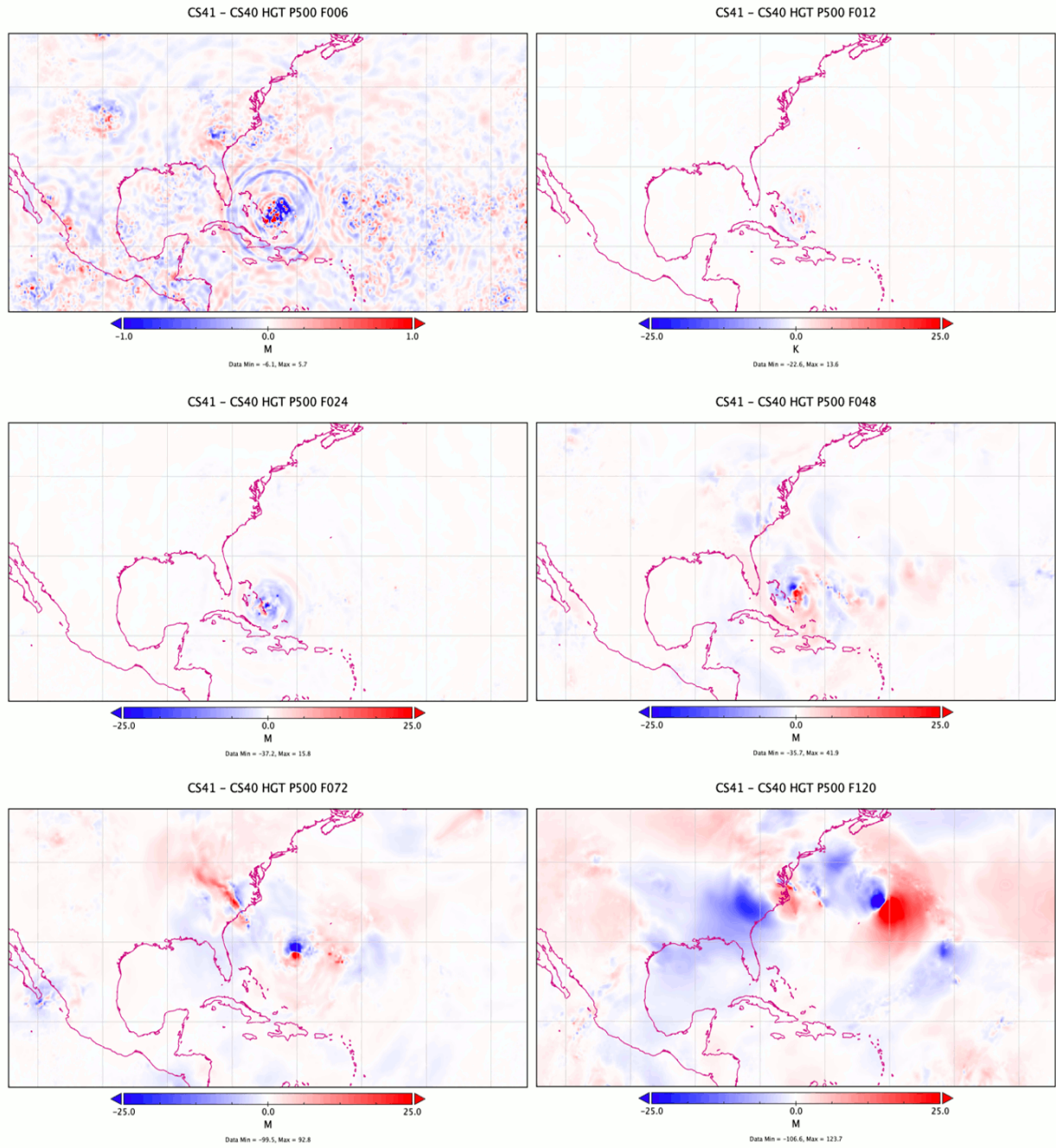


Figure 15. As in Figure 14, but for 500 hPa geopotential height (in m).

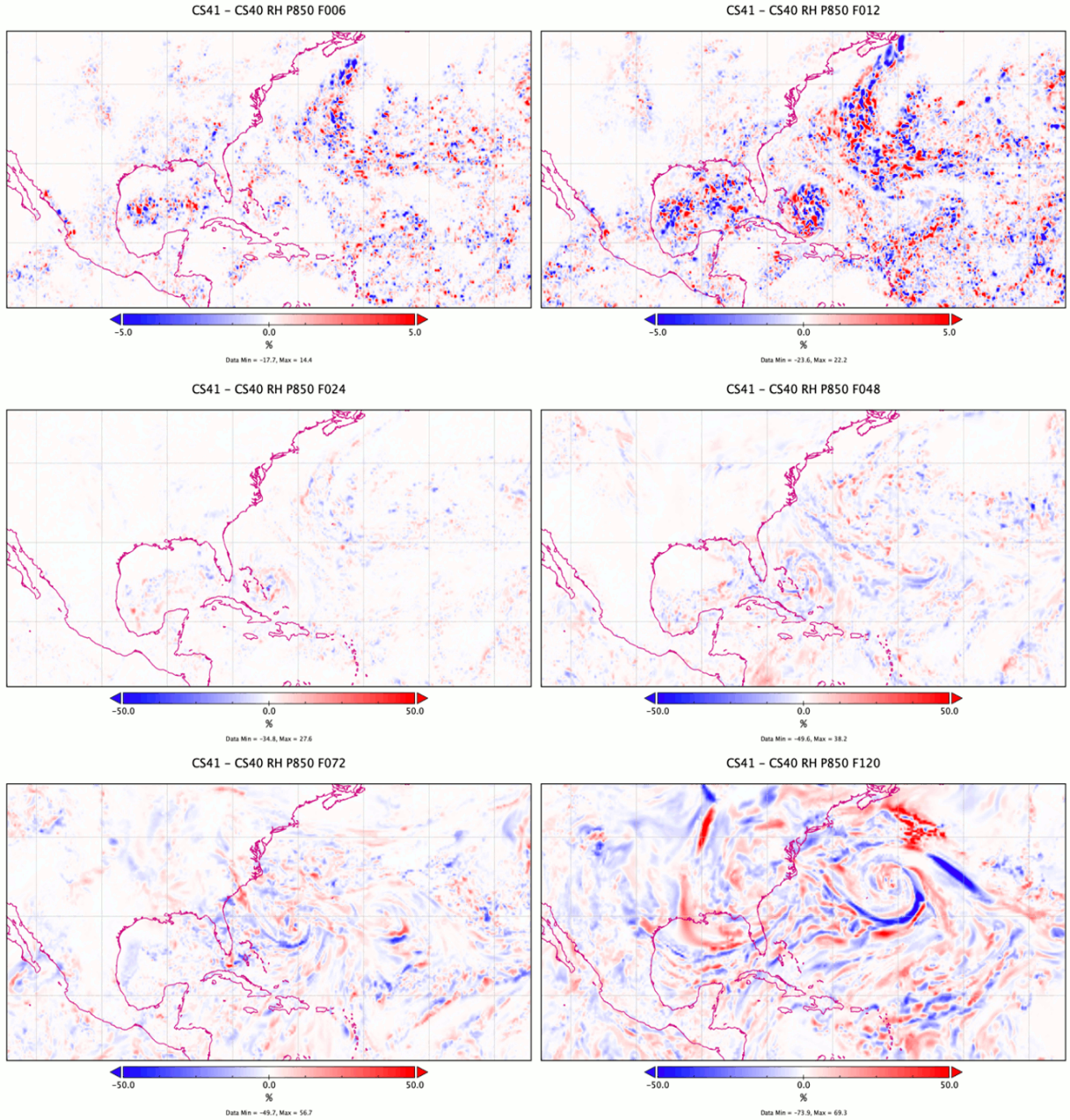


Figure 16. As in Figure 14, but for 850 hPa relative humidity (in percent). Note the change in the color scale starting at 24 hours (center left panel).

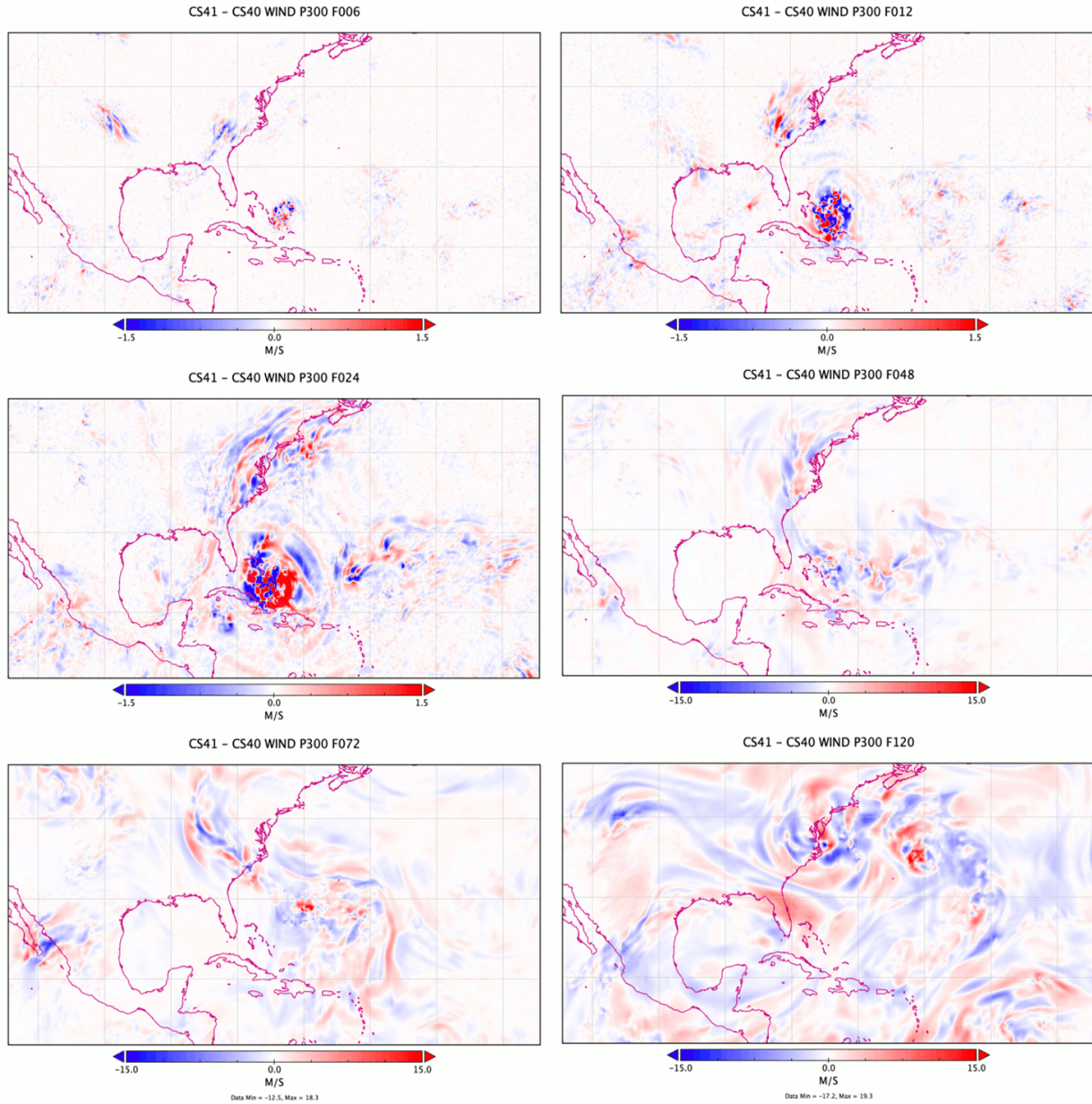


Figure 17. As in Figure 14, but for 300 hPa wind speed (in m/s). Note the change in the color scale starting at 48 hours (center right panel).

3.3.5 Analysis of Difference Fields Between Cloud Overlap Simulations

This section summarizes the most prominent aspects of the time series of several model difference fields from the H220 cold start Joaquin simulations. The cloud overlap configurations are identified as follows in the nine figures in this section (Figures 14-22): 1) “CS40”; EXP overlap with constant decorrelation length, Z_0 , 2) “CS41”; EXP overlap with varying Z_0 , 3) “CS50”; ER overlap with constant Z_0 , and 4) “CS51”; ER overlap with varying Z_0 . Figures 14-17 show predicted difference fields at various forecast times between CS41 and CS40 to highlight the

impact of the decorrelation length approach for 850 hPa temperature in K (Figure 14), 500 hPa geopotential height in meters (Figure 15), 850 hPa relative humidity in percent (Figure 16), and 300 hPa wind speed in m/s (Figure 17). Figures 18-21 show predicted difference fields at various forecast times between CS50 and CS40 to highlight the impact of the cloud overlap method for 850 hPa temperature in K (Figure 18), 500 hPa geopotential height in meters (Figure 19), 850 hPa relative humidity in percent (Figure 20), and 300 hPa wind speed in m/s (Figure 21).

Initially, at forecast hour 6, the cloud overlap treatments manifest themselves as expected at the grid scale, with numerous grid points exhibiting small differences. The patterns and magnitudes are similar between the EXP and ER overlap approaches (Figures 18-21) and between different Z_0 formulations (Figures 14-17). Over the first 24 forecast hours, these small-scale features grow upscale and over the remainder of the forecast period substantially influence the meso- and synoptic-scale environmental fields.

During the first 12 hours, there is a period of dynamical adjustment (presumably) from areas of convection that is facilitated by outward propagating gravity waves that are at least partly caused by the differing initialization procedures for the environment and the vortex. These are quite evident, for example, in the height field at 6 hours for the CS41 minus CS40 comparison in Figure 15. The rings of alternating positive and negative differences are present in several large-scale features, including Hurricane Joaquin and convection over the southeastern United States. The change in scale at 12 hours minimizes the widespread relatively small magnitude differences and emphasizes the impact of the cloud overlap approaches on the vigorous convection associated with Joaquin.

By hour 72 in the CS50 minus CS40 comparison, relatively large differences appear in two areas: The first is the dipole associated with the position of Joaquin, while the second appears to be related to the positioning of the rainband that is oriented northwest-southeast along the coast of the Carolinas (see, e.g., the 500 hPa height differences at 72 hours in Figure 19). The CS50 run positioned the trough (and likely the moisture stream) farther northeast. Similar differences in the position of these features are also seen in the CS41 minus CS40 comparison (see Figure 15). It should be mentioned that this feature resulted in excessive observed rainfall amounts (>500 mm) and extensive flooding. *Marciano and Lackmann (2017)* in a numerical study demonstrated using potential vorticity inversion that the locations of the onshore flow and the upper-low were influenced by the latent heating (i.e., downstream ridge building) associated with Hurricane Joaquin. The inclusion of additional plots of 500 hPa height at 84 and 96 hours for this case (Figure 19) illustrates the substantial modifications to the height field in the vicinity of the upper low, with a prominent dipole at 120 hours suggesting that the low was positioned farther west in the CS50

simulation. The broad area of higher heights in the CS50 simulation near Joaquin indicates synoptic-scale changes to the height field by this cloud overlap approach. Indeed, this simulation resulted in a storm track that did not exhibit a bend to the northwest and may indicate that there was less influence – via a Fujiwhara interaction – from the upstream upper-low.

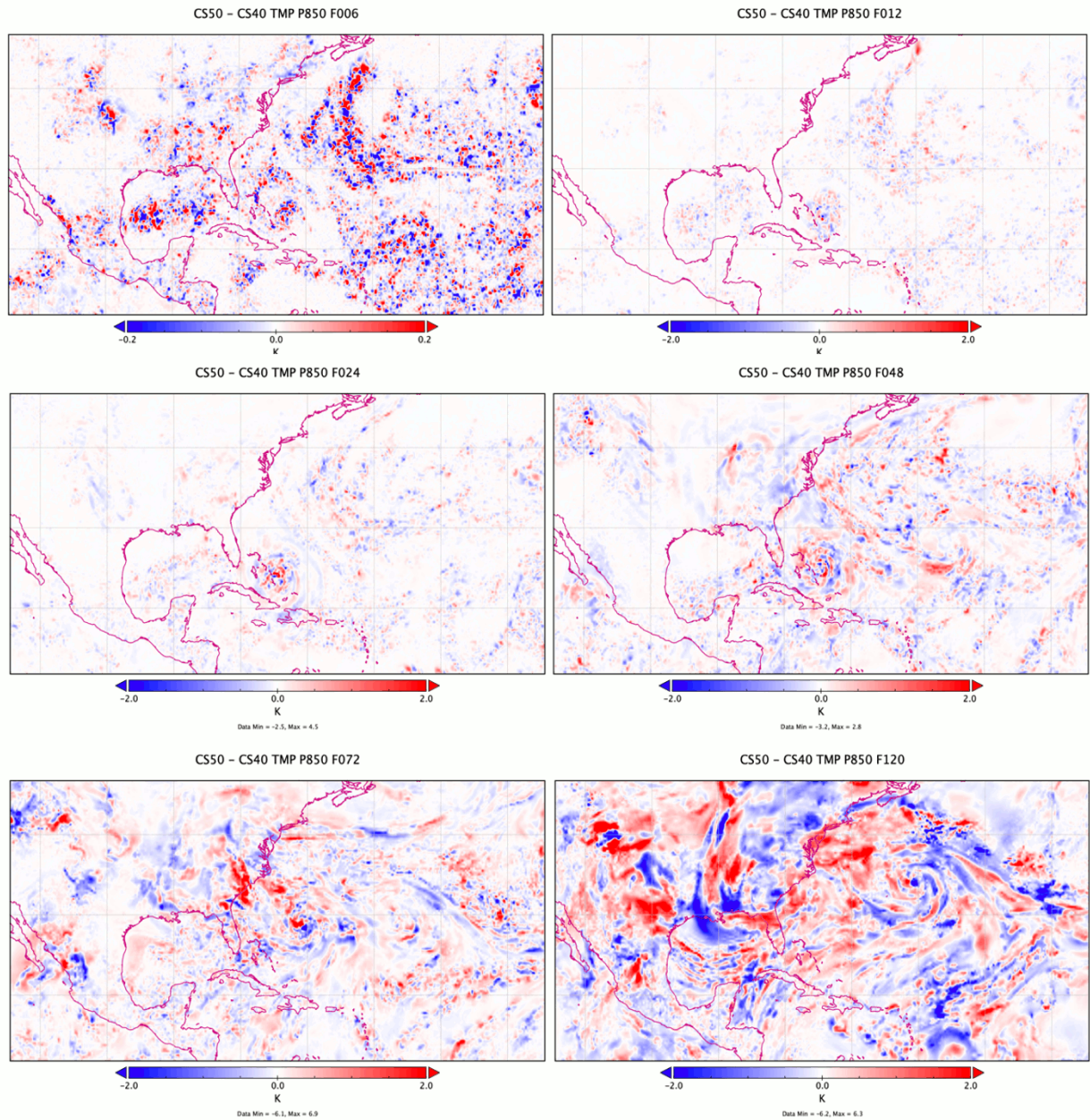


Figure 18. MET-generated differences in H220 predicted 850 hPa temperature (in K) for a forecast cycle initialized at 00 UTC 1 October 2015 of Hurricane Joaquin between model runs using ER cloud overlap with constant decorrelation length “CS50” and EXP cloud overlap with the same constant decorrelation length “CS40” at six forecast times. Note the change in the color scale between the plot at forecast hour 06h and the later forecast times.

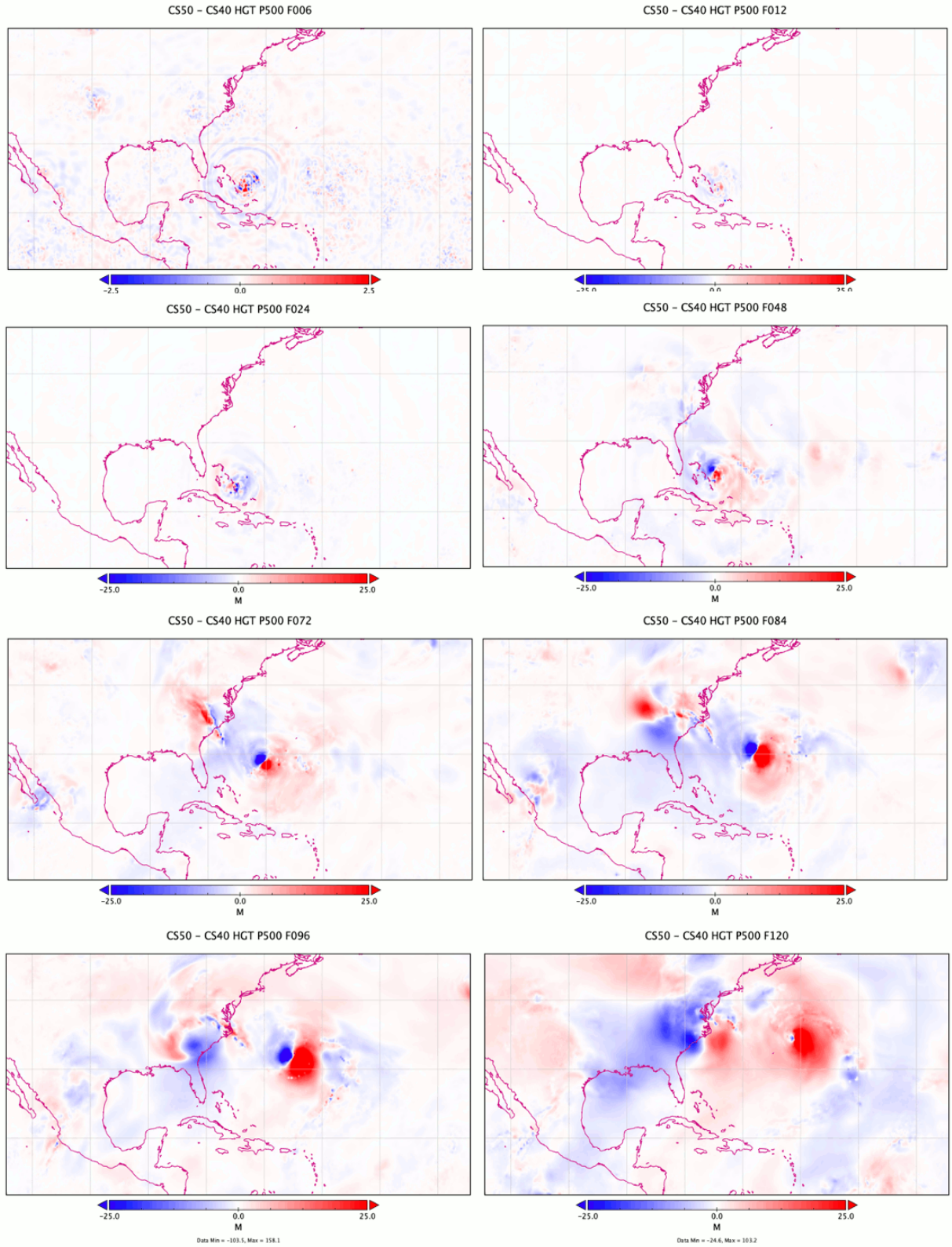


Figure 19. As in Figure 18, but for 500 hPa geopotential height (in m) at eight forecast times. Note the change in the color scale between the plot at 6 hours (top left) and the later forecast times.

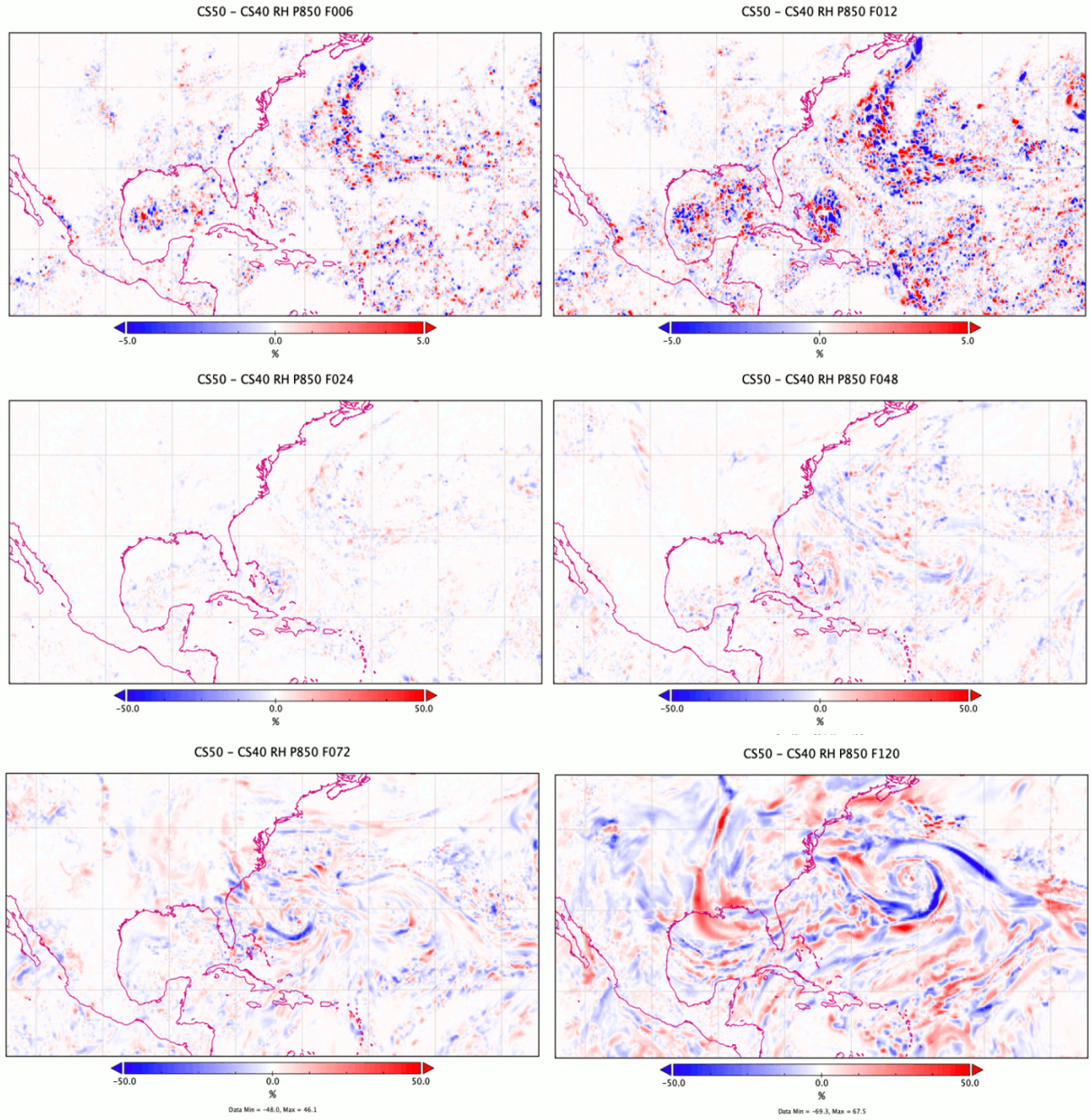


Figure 20. As in Figure 18, but for 850 hPa relative humidity (in percent). Note the change in the color scale between the first two forecast times (top panels) and the later forecast times.

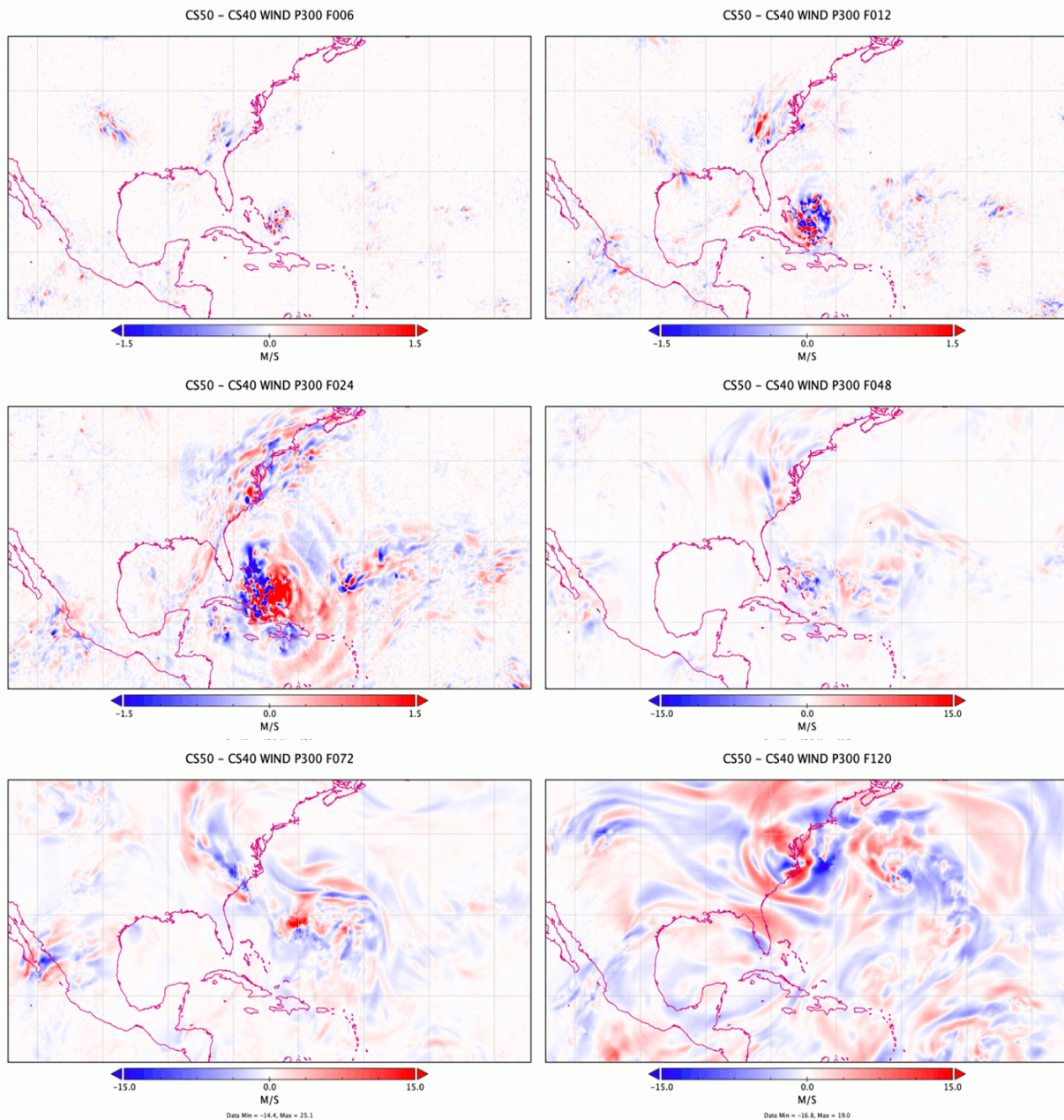


Figure 21. As in Figure 18, but for 300 hPa wind speed (in m/s). Note the change in the color scale starting at 48 hours (center right panel).

The upper-level 300 hPa wind field shows pronounced sensitivity to the cloud overlap selection in the vicinity of Joaquin and the upper low (Figure 21). At shorter time ranges, areas near upper-level jet streaks and regions of precipitation over the East Coast of the US (compare with Figure 4 of *Marciano and Lackmann, 2017*) are favored regions of sensitivity. A multitude of individual small-scale features in the areas of sensitivity begin to aggregate upscale at longer forecast ranges and, while initially collocated with the upper low and Joaquin, begin to spread downstream at farther distances from the features at longer forecast lengths.

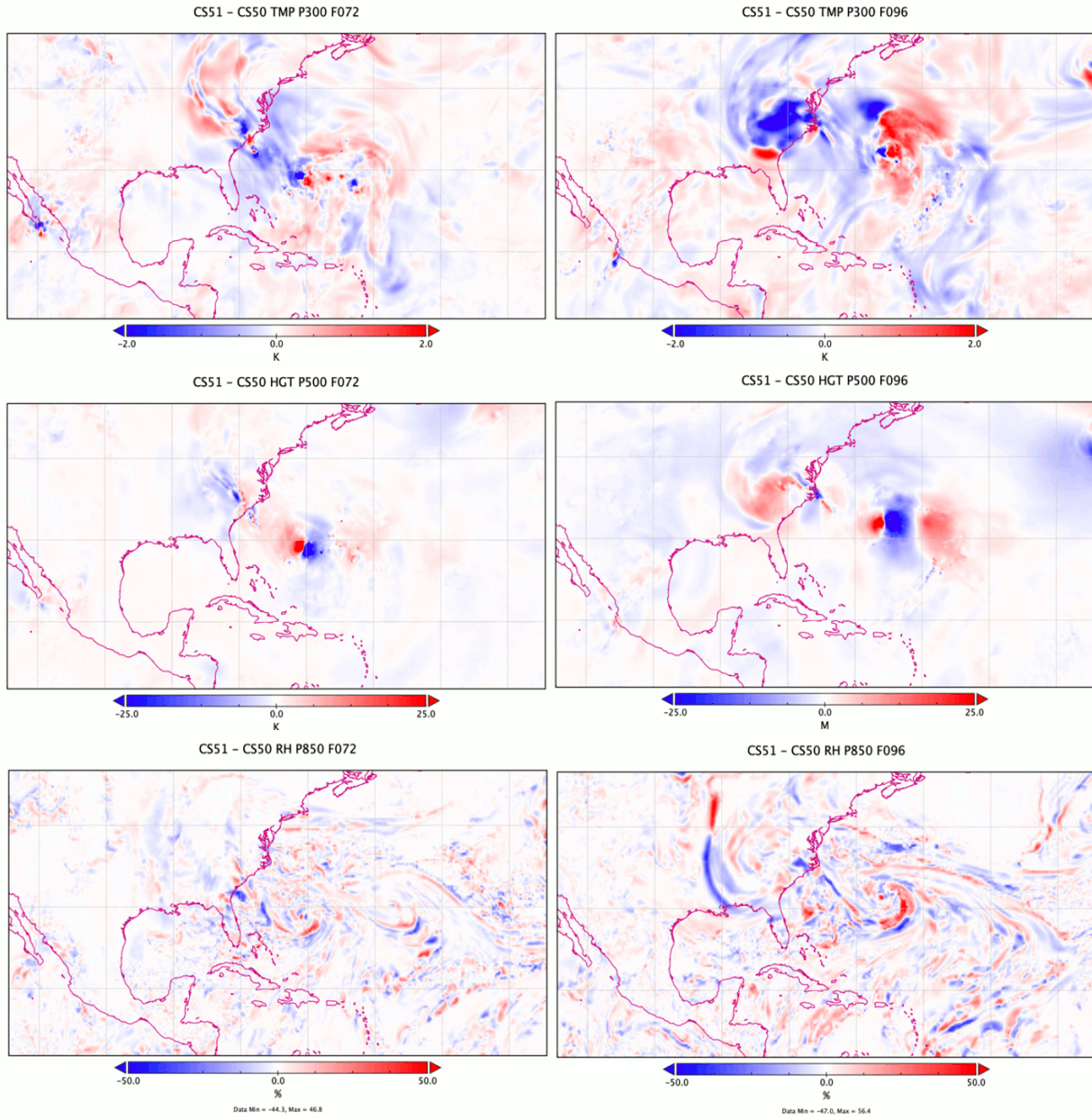


Figure 22. MET-generated 72-hour and 96-hour differences in H220 predicted 300 hPa temperature (top row), 500 hPa geopotential height (center row), and 850 hPa relative humidity (bottom row) for a forecast cycle initialized at 00 UTC 1 October 2015 of Hurricane Joaquin between model runs using ER cloud overlap with varying decorrelation length “CS51” and ER overlap with constant decorrelation length “CS50”.

The final set of plots, in Figure 22, shows the 72- and 96-hour 300 hPa temperature (top row, in K), 500 hPa height (middle row, in meters), and 850 hPa relative humidity (bottom row, in percent) difference fields for CS51 minus CS50. At these times, Joaquin began the most pronounced bend to the left (north) of any CS51 cold start run, while Joaquin continued its straight trajectory to the northeast in CS50 (unique in this set of four cold start runs). Forecast differences due solely to position differences appear as red/blue dipoles. The fields exhibit substantial changes

between 72 and 96 hours, with an increase in the magnitude and spatial extent of the differences especially downstream of Joaquin. The CS51 simulation has higher heights at 500 hPa east of Joaquin, as well as a broad area of warmer temperatures at higher altitudes at 300 hPa. The relative humidity field difference shows a circular band of higher values in the CS51 run, perhaps indicative of enhanced convection that would support the higher heights and temperatures immediately downstream. While details are lacking from this preliminary analysis, these features might suggest a possible contribution to the farther northwest track seen in CS51.

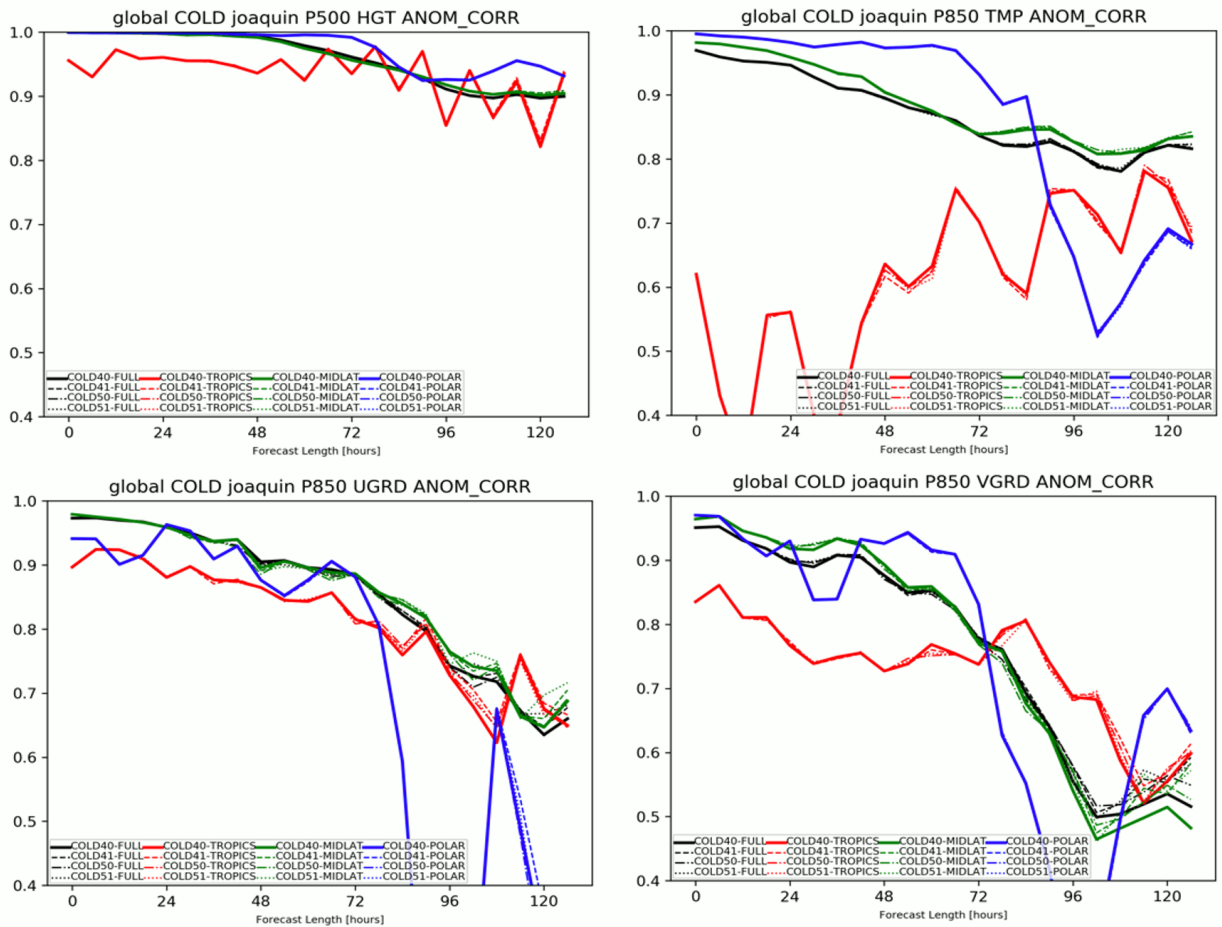


Figure 23. Anomaly correlation of 500 hPa height (top left), 850 hPa temperature (top right), 850 hPa u-wind (bottom left) and 850 hPa v-wind (bottom right) as a function of forecast hour from H220 cold start predictions of Hurricane Joaquin averaged over the full domain (black) and over tropical (red), mid-latitude (green), and polar (blue) latitudes for a matrix of four cloud overlap and decorrelation methods (line styles).

3.3.6 Analysis of Domain-wide Statistics

This section discusses anomaly correlation (ANOM_CORR) and mean error (ME) statistics generated with the “grid_stat” component of MET for the cold start H220 Joaquin predictions for the matrix of four cloud overlap and decorrelation length configurations. The mean error – for the single cycle studied here – represents the simple difference between the experiments

when averaged over the domain. The anomaly correlation values are noisy since they are similarly based on only one cycle. Error statistics generally degrade with forecast length as expected. Figure 23 shows the anomaly correlation for 500 hPa geopotential height (top left), 850 hPa temperature (top right), 850 hPa zonal wind speed (bottom left), and 850 hPa meridional wind speed (bottom right) for the full domain average (in black), and for averages over tropical (red), mid-latitude (green), and polar (blue) latitudes for the four cloud overlap configurations (differing line styles). As before, the tropical band extends from 20° S to 20° N, the mid-latitude band extends from 20-60° N, and the polar band is poleward of 60° N within the d01 grid. Figure 24 shows the mean errors for the same parameters and spatial averages as in Figure 23. In general, there is very little influence by the choice of cloud overlap treatment on either the domain-wide mean error or anomaly correlation until later in the forecast runs, especially at 96 and 120 hours. The largest effect is on the u- and v- wind components at these long forecast ranges, and considerable variations are also noted in the statistics among the plotted regions.

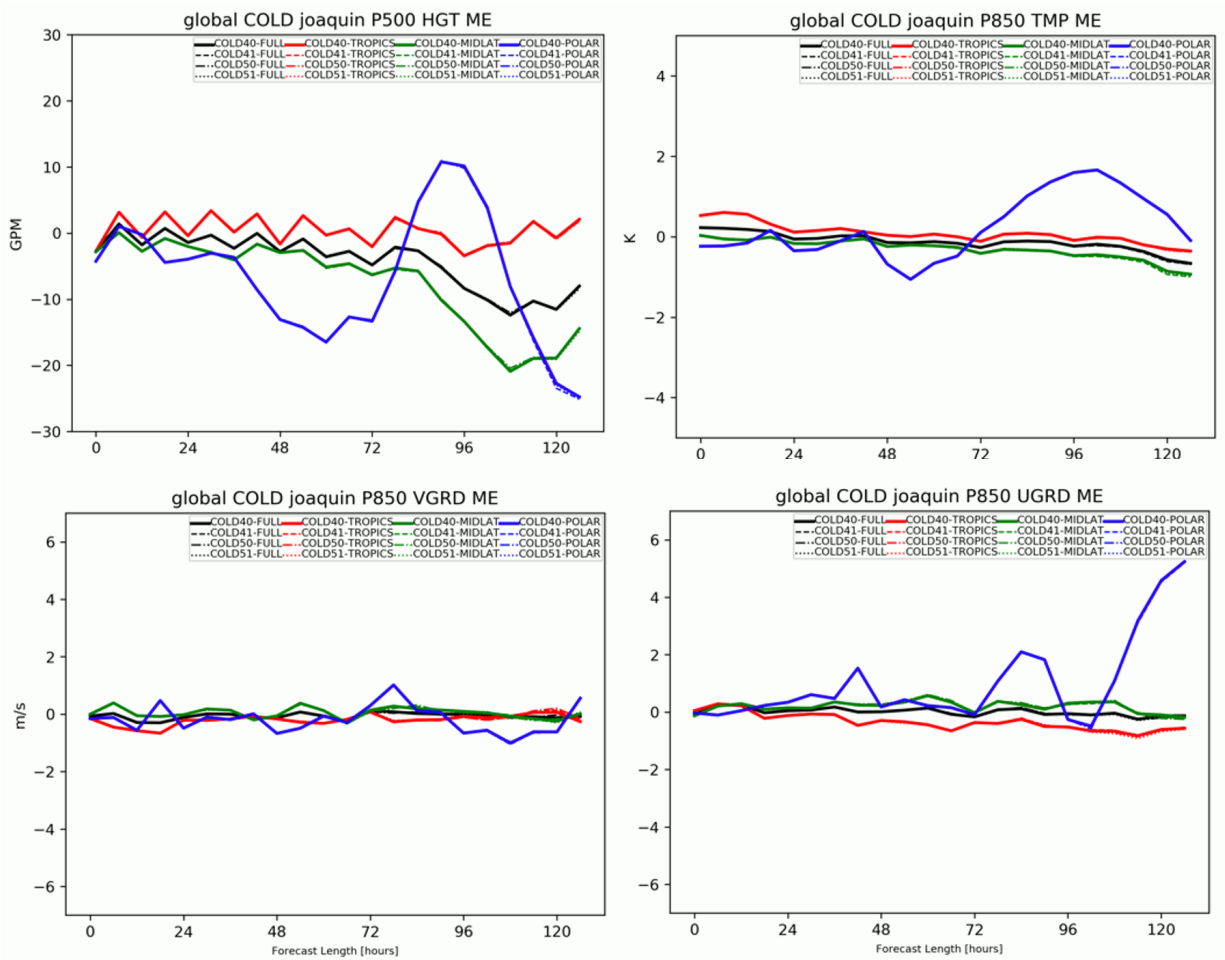


Figure 24. Mean errors of 500 hPa height (top left), 850 hPa temperature (top right), 850 hPa u-wind (bottom left) and 850 hPa v-wind (bottom right) as a function of forecast hour from H220 cold start predictions of Hurricane Joaquin averaged over the full domain (black) and over tropical (red), mid-latitude (green), and polar (blue) latitudes for a matrix of four cloud overlap and decorrelation methods (line styles).

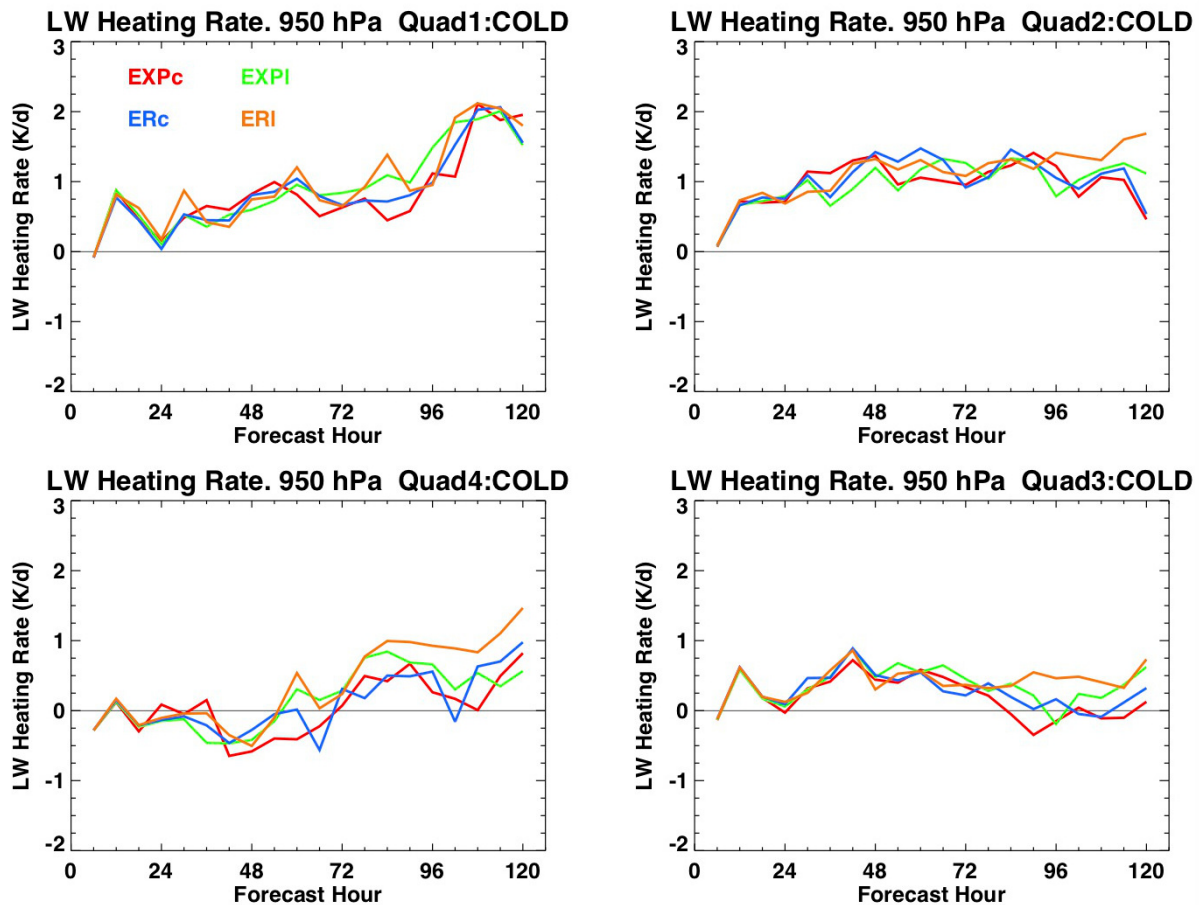


Figure 25. Quadrant mean 950 hPa longwave heating rate from H220 cold start predictions of Hurricane Joaquin for runs initialized at 00 UTC on 1 October 2015 averaged over the d03 inner grid spatial quadrants to the northwest (top left), northeast (top right), southwest (bottom left) and southeast (bottom right) of the storm center for the two cloud overlap methods with constant decorrelation length (EXPC and ERc) and with latitude varying decorrelation length (EXPI and ERI).

3.4 H220 Testing: AER Joaquin Spatial Mean Heating Rates

A final analysis of the H220 Joaquin runs was completed to examine quadrant mean heating rates to demonstrate the sensitivity of low-level radiative heating rate in the vicinity of the TC to the cloud overlap and decorrelation length methods within the d03 storm-centered inner grid. Figure 25 shows the time series of 950 hPa longwave radiative heating rate from the cold start runs averaged over grid cells to the northwest (top left), northeast (top right), southwest (bottom left), and southeast (bottom right) of the storm center for the two cloud overlap methods with constant decorrelation length (“EXPC” and “ERc”) and with latitude varying decorrelation length (“EXPI”, and “ERI”). Figure 26 shows comparable quadrant mean longwave heating rate time series from the warm start Joaquin simulations. Positive longwave heating rates represent strongly absorbing and emitting clouds and convective areas, while negative values represent more

clear sky and less convective areas. These plots illustrate the evolution of low-level clouds and convection within each quadrant and its sensitivity to the cloud overlap configurations and the specification of the initial conditions. Noticeable differences include a tendency for more cloud-induced heating rate in the southwest quadrant of the warm start runs relative to the cold start runs, especially after 48 hours, possibly due to the greater storm intensity in the warm start runs. Both the cold and warm start runs show significant influence of clouds on the radiative heating to the northwest and northeast of the center with somewhat more cloud overlap sensitivity in the warm start runs in these quadrants. The southeast quadrant shows smaller heating rates in both the cold and warm start runs, suggesting somewhat less convection in that part of the storm during this forecast cycle.

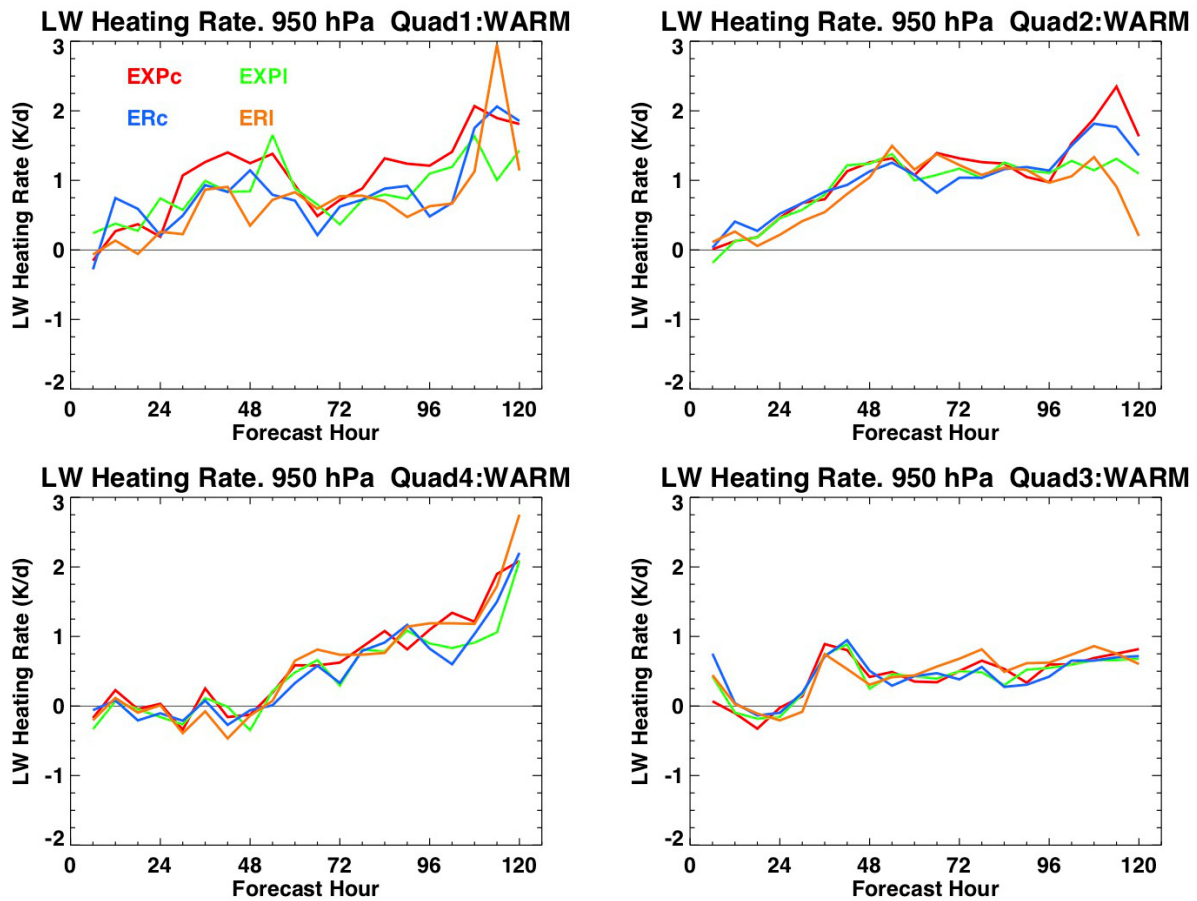


Figure 26. Quadrant mean 950 hPa longwave heating rate from H220 warm start predictions of Hurricane Joaquin for runs initialized at 00 UTC on 1 October 2015 averaged over the d03 inner grid spatial quadrants to the northwest (top left), northeast (top right), southwest (bottom left) and southeast (bottom right) of the storm center for the two cloud overlap methods with constant decorrelation length (EXPc and ERc) and with latitude varying decorrelation length (EXPl and ERI).

3.5 RRTMG Radiation Differences within the NOAA Modeling Applications

An additional task of this project was to assess differences among the primary applications of the RRTMG radiation code being used in NOAA operations to inform a decision by NOAA on which form of the radiation code is the optimal one to apply to the UFS. Several points of historical background are relevant to this investigation. First, the version of RRTMG in GFS_v16 was originally implemented about twenty years ago and was significantly adapted and stylistically altered by NOAA for optimal application to the global model and to the computer systems that are used to run GFS operationally. Second, the version of RRTMG that is currently distributed in WRF (and used within HWRF) was originally implemented by the PI (Iacono) at AER and first released in Version 3.1 of the Advanced Research WRF (ARW) in 2009. This version of RRTMG largely retains the form in which it is publicly released by AER on github with modifications to combine numerous modules and source code files into two consolidated source files for the longwave and shortwave components and to adapt the radiation interfacing for ARW. An important consequence is that RRTMG followed different development paths over the last ten to twenty years between GFS and ARW since their original implementations. Using recent versions of GFS, WRF, and HWRF, we have examined the state of the radiation code used in each of these models to document and to resolve any scientific discrepancies of importance to the future application of RRTMG in the Hurricane Analysis and Forecasting System (HAFS) application of the UFS.

This code comparison was performed during late 2019 and early 2020 and examined the state of the radiation code and interfacing in WRF_ARW_v4.0, HWRF_v4.0a, and GFS_v16. In general, although the application of RRTMG within each of these dynamical models began using different versions of the radiation code at different times and each has evolved substantially over the years, this analysis has determined that each application has remained current with the major updates and fixes released by AER through 2019. A detailed list of differences in radiation coding and interfacing among WRF, HWRF and GFS is provided in Table A1 in the Appendix (Section 6) including descriptive footnotes. The primary conclusions of this analysis are listed below.

- Despite the significant stylistic differences between the state of the radiation code in WRF/HWRF and GFS and their very different development paths and applications, the major scientific components are functionally similar and updated relative to AER public releases of RRTMG except for the most recent radiation enhancements (see Table A1).
- Although they relate to the specification of model inputs rather than the radiation source code itself, multiple differences are noted in the radiation input interfaces in WRF/HWRF and GFS applications that may nevertheless affect the accuracy of radiative flux and heating rate calculations, though establishing this impact is beyond the scope of this work.

- The recent addition of the EXP and ER cloud overlap treatments and the associated decorrelation length methods (released by AER as RRTMG_LW_v5.0 and RRTMG_SW_v5.0) have been implemented in HWRF and are available (through CCMPP-physics) to GFS and UFS, though they have not been implemented in the public release of ARW as of summer 2021. As a result, WRF-ARW continues to apply maximum-random cloud overlap in the RRTMG radiation option, HWRF has both EXP and ER available (the operational HWRF uses ER cloud overlap with a constant decorrelation length of 2500 m), and GFS_v16 uses an alternate version of EXP cloud overlap implemented by NOAA with a spatially varying decorrelation length acquired from ECMWF.
- The updated solar source function and solar variability option added to RRTMG_SW_v4.0 and updated in v4.1 have not been added to any of WRF, HWRF, or GFS/UFS as of summer 2021. This change also provides a reduction in the default solar constant used in RRTMG_SW from the previous value of 1368.2 Wm⁻² to a new value of 1360.85 Wm⁻², which is closer to recent TSI observations. These solar options are of highest relevance to climate simulations and may be a lower priority for weather predictions.
- WRF and HWRF typically use a model top pressure in the stratosphere near 5-20 hPa, although this boundary level can be specified by the user. Since some absorption and emission, particularly in the longwave, occurs above this level, the resulting radiative transfer will be slightly deficient. Methods are in place in WRF and HWRF to offset this discrepancy by adding an additional layer (in the SW) or layers (in the LW) within the radiation calculation to approximate radiative absorption and emission above the model top. GFS_v16 recently switched to a much higher model top near 80 km (< 0.01 hPa), which avoids this issue.
- The effective vertical limit of accurate heating rate calculations provided by RRTMG (and RRTMGP) is approximately 0.05-0.1 hPa, and degraded results should be expected above this level. The recently raised model top in GFS_v16 introduces potential radiative heating discrepancies in the highest model layers. AER is currently developing modifications for both RRTMG and RRTMGP to increase the accuracy of heating calculations in the mesosphere and lower thermosphere up to about 100 km.

4. Conclusions and Future Work

This DTC Visitor Program project advanced our investigation of enhancements to the cloud overlap and decorrelation length methods used in the RRTMG radiation code within NOAA operations in the context of HWRF hurricane predictions. Based on our earlier efforts, NOAA adopted the EXP cloud overlap method with constant decorrelation length in the 2018 operational HWRF model. For this project, DTC and AER performed and analyzed multiple tropical cyclone

experiments, in collaboration with EMC, to evaluate the impact on TC track and intensity predictions of the ER cloud overlap treatment and additional related enhancements. In some TC cases, modest improvement in bias and track errors and other statistics was shown for the ER method relative to the baseline configuration using EXP. In part due to this analysis, NOAA decided to adopt the ER cloud overlap method with constant decorrelation length within the 2020 operational HWRF model.

The ability to predict the movement of Hurricane Joaquin with skill in real time was limited due to its very unusual track and the factors that influenced it. Model predictions of this case remain very sensitive to model configuration. This TC was studied in some detail during this project to examine its response and sensitivity to the cloud overlap enhancements. New simulations of Joaquin using the pre-implementation version of H220 were completed by DTC using both cold start and warm start initial conditions and a set of four cloud overlap configurations. The evolution of Joaquin in these runs was shown to be sensitive to the type of initialization and the application of forecast cycling with the warm start runs more closely matching the sharp recurvature of the track observed during the initial days of the forecast cycle examined as well as the northeastward movement later in the cycle. Furthermore, both the track and intensity were shown to be sensitive to the cloud overlap and decorrelation length method used.

This study also examined the substantial differences in the RRTMG coding among the WRF, HWRF and GFS models. The code differences were found to be mostly stylistic or related to improving computational efficiency, or they were connected to variations in the specification of model inputs. The scientific aspects of the radiation codes were found to be closely aligned. An exception is the application of radiation code updates released by AER since 2019. Specifically, although the EXP and ER cloud overlap methods are available in HWRF (due to our efforts for the DTC) and are available to GFS and UFS through the CCPP (through our efforts supported by NOAA), these enhancements are not yet available in the WRF ARW public release. This report concludes that the version of RRTMG in the GFS is the most appropriate choice for application to CCPP and UFS, until such time that the updated RRTMGP radiation code is selected to replace it.

There are several directions in which this work can be continued in the future. First, the new cloud overlap methods have not been tested in the context of TC prediction in HAFS, and we will consider proposing a new DTC/VP project for this task. In addition, our ongoing efforts for NOAA include testing new physics enhancements. These include expanding the representation of sub-grid cloud variability by treating the vertical overlap of cloud condensate using a method like that used for cloud overlap and improving the coupling of radiation to both microphysics and surface properties, and we will investigate these topics in the context of hurricane predictions.

5. Project Deliverables

This project generated several code related deliverables and supporting documents (including this final project report) for the DTC and NOAA including:

- 1) Source code for the exponential and exponential-random cloud overlap methods and the constant and latitude-varying decorrelation length treatments was implemented into RRTMG in CCPP, and these changes were subsequently pulled into the NCAR master CCPP repository during 2020, though this occurred too late for these changes to be included in the CCPP_v5.0 release.
- 2) The previously delivered exponential-random cloud overlap source code was adopted by NOAA/EMC during this project for operational use in HWRF for the 2020 hurricane season during Spring 2020.
- 3) A script written by John Henderson that uses the MET “Series-Analysis” tool to generate field map graphics was provided to DTC. This script is publicly available at https://www.dtcenter.org/sites/default/files/communitycode/hwrf/developers/codes/series_analysis.tar.gz.
- 4) A document detailing the comparison between the RRTMG source codes in the WRF and GFS models was provided to DTC and presented during a virtual meeting with DTC on April 22, 2020.
- 5) Iacono, M.J., and J.M. Henderson, Testing exponential-random cloud overlap for HWRF operations and unifying RRTMG radiation codes in operational use at NOAA, 2019-2020 DTC Project Final Report, Developmental Testbed Center, August 2021.

In addition, multiple presentations were delivered during this project, including two posters (at AMS Conferences), two invited EMC seminars, and a project review summary at the 2020 NOAA OSTI PI Meeting, which included elements of this research:

- 1) Iacono, M.J., and J. Henderson, Cloud overlap radiation enhancements for tropical cyclone prediction with HWRF, Invited seminar for the NOAA Environmental Model Center (EMC) Hurricane Team, September 5, 2019.
- 2) Iacono, M.J., J.M. Henderson, L. Bernardet, E. Kalina, M. Biswas, K. Newman, B. Liu, and Z. Zhang, Enhancements to cloud overlap radiative effects for weather forecasting and tropical cyclone predictions, Poster presentation at the American Meteorological Society Tropical Meteorology and Tropical Cyclones Symposium, 100th AMS Annual Meeting, Boston, Massachusetts, January 12-16, 2020.
- 3) Iacono, M.J., and J. Henderson, Sub-grid cloud overlap radiation enhancements for UFS global weather forecasting and tropical cyclone prediction, Virtual presentation for the NOAA OSTI Principal Investigator Meeting, July 30, 2020.
- 4) Iacono, M.J., E. Mlawer, J. Henderson, and G. Thompson, Radiation enhancements for UFS global weather predictions, Invited virtual seminar for the NOAA Environmental Modeling Center, Modeling and Data Assimilation Branch, Physics Group Bi-Weekly Meeting, October 22, 2020.
- 5) Iacono, M.J., J. Henderson, L. Bernardet, E. Kalina, M. Biswas, K. Newman, B. Liu, and Z. Zhang, Enhancements to cloud overlap radiative effects for tropical cyclone prediction, Poster presentation at the 34th American Meteorological Society Conference on Hurricanes and Tropical Meteorology, Virtual Meeting, May 10-14, 2021.

6. Appendix

Table A1 lists details of the RRTMG_LW and SW source code comparisons for the models as they are used in WRF_v3.8, HWRF_v4.0a and GFS_v16. Footnotes with additional details that are identified by numbers in parentheses are listed after Table A1.

Table A1. RRTMG source code differences among WRF, HWRF and GFS.

| Category | WRF_ARW_v3.8 | HWRF_v4.0a (DTC 2018) | GFS_v16 / UFS-fv3atm |
|--|---|-------------------------------------|---|
| Code Comparison | | | |
| General Code State | Close to AER release (1) | Close to AER release (1) | Significantly modified from AER release (2) |
| Original RRTMG Version Implemented | LW_v4.71 SW_v3.7 | LW_v4.71 SW_v3.7 | Before LW_v4.0 Before SW_v3.6 |
| Current Equivalent RRTMG Version | LW_v4.85 (3) SW_v4.02 (4,5) | LW_v4.85 (3) SW_v4.02 (4,5) | LW_v4.85 (3) SW_v4.02 (4,5) |
| Cloud Overlap Methods Available | MR | MR, EXP, ER (6) | MR, EXP (7) |
| Missing LW Features in Latest AER Releases (LW_v5.0) | Yes (8) | No | Yes (8) |
| Missing SW Features in Latest AER Releases (SW_v5.0) | Yes (9) | Yes (9) | Yes (9) |
| Random Number Generator | “kissvec” (10) | “kissvec” (10) | Mersenne Twister (10) |
| Radiation Treatment Above Model Top Pressure | LW: Extra layers SW: Extra layer | LW: Extra layers SW: Extra layer | None; Model top in mesosphere |
| Radiation Frequency | | | |
| Interval Between Full Radiation Calls | 30 minutes (default); same value all nests (11) | Domain and time step dependent | 60 minutes (default) |
| Input Data | | | |
| CO2 VMR Amount | 379.e-6 | 379.e-6 | 350.e-6 (12) |
| CH4 VMR Amount | 1774.e-9 | 1774.e-9 | 1500.e-9 |
| N2O VMR Amount | 319.e-9 | 319.e-9 | 310.e-9 |
| CO VMR Amount | 0.00 | 0.00 | 15.e-9 |
| Ozone Specification | CAM climatology (default) | Uses GFS ozone profiles | Interactive ozone profile, or Moorthi ozone climatology |
| CFC11 VMR Amount | 0.251e-9 | 0.251e-9 | 0.352e-9 |

| | | | |
|---------------------------------|---|---|--|
| CFC12 VMR Amount | 0.538e-9 | 0.538e-9 | 0.6358e-9 |
| CFC22 VMR Amount | 0.169e-9 | 0.169e-9 | 0.150e-9 |
| CCL4 VMR Amount | 0.093e-9 | 0.093e-9 | 0.1397e-9 |
| O2 VMR Amount | 0.209488 | 0.209488 | 0.209 |
| Clouds | Liquid: Hu & Stamnes Ice: Fu Rain: TBD Snow: TBD | Liquid: Hu & Stamnes Ice: Fu Rain: TBD Snow: TBD | Liquid: Hu & Stamnes Ice: Fu Rain: CAM formula Snow: Fu |
| Cloud Fraction Parameterization | User selectable | User selectable | |
| Aerosols | WRF_ARW: Climo WRF-Chem: Yes | Not used | Yes; Tropospheric climatology, and parameterized in stratosphere |

RRTMG Code Review Footnotes:

(1): The code formatting in WRF and HWRF is similar to the form of the AER releases, though the multiple source files have been combined into two single source file modules for LW and SW, each containing a new interface routine for connection to the WRF radiation driver.

(2): The GFS code formatting is substantially revised from the AER releases for consistency with the GFS coding style, though the science is consistent with the AER release versions listed. Value of the GFS coding style going forward for CCPP depends on:

- a) Coding style preferences for UFS/CCPP,
- b) Relevance of GFS customizations to performance on specific computer hardware
- c) Intended target computer hardware for UFS/CCPP and whether revisions are still needed

(3): LW does not include dF/dT derivative option added in v4.84 (used to estimate change in vertical profile of upward flux as a function of surface temperature at model time steps between full radiation calls)

(4): SW does not include solar variability option (following the NRLSSI2 solar model) added in v4.0 and fixed in v4.1. This capability allows several options:

- a) Use fixed solar source function with no solar variability
- b) Updated solar constant = 1360.85 Wm⁻² (former Kurucz value was 1368.22 Wm⁻²)
- c) Model average solar variability with mean solar cycle
- d) Model specific solar cycle through input of facular and sunspot indices

(5): In source file “module_ra_rrtmg_sw.F”, in module cldprmc_sw, lower bound of IF check on radliq (when liqflag = 1) should be changed from 1.5 to 2.5

(6): EXP and ER cloud overlap as added by Iacono and Henderson (AER); includes both constant decorrelation length and day-of-year and latitude-varying decorrelation length that varies from 1.4 near poles to 3.6 at low latitudes following the peak sun during the year

(7): EXP cloud overlap as added by Yu-Tai Hou (EMC); includes latitude-only varying decorrelation length (obtained from ECMWF) with values that range from 0.6 at the poles to 2.8 at the equator. Previously operational GFS_v15 used only MR overlap with RRTMG

(8): Missing EXP and ER cloud overlap as added by AER; new overlap methods provided to EMC for GFS through CCpp; not yet provided to NCAR for WRF

(9): a) Missing EXP and ER cloud overlap as added by AER (WRF and GFS); new overlap methods provided to EMC for GFS; not yet provided to NCAR for WRF

b) Missing updates to three solar input data components used by new solar variability capability (not currently used by GFS, WRF, or HWRF)

c) Missing correction to LAYREFFR from 58 to 42 in band 28; increases SW heating rate by about 0.1 K/day near 1 hPa

d) Missing revision to calculation of “zwo” in module rrtmg_sw_reftra.f90 to avoid unlikely divide by zero condition

(10): a) “kissvec” method originally obtained for RRTMG from NCAR/CAM;

b) “Mersenne Twister” method originally obtained for RRTMG from Robert Pincus; later adapted for GFS from original source material by Mark Iredell (NOAA)

c) Results may not be identical between the two methods, but will be statistically unbiased when used with McICA in RRTMG

(11): WRF User Guide recommends a radiation frequency in minutes = grid size in km (e.g. 10 min for 10 km)

(12): GFS trace gas amounts listed may be only default values that are replaced operationally by more recent values

7. References

- Barker, H., J.N.S. Cole, J.-J. Morcrette, R. Pincus, P. Raisanen, Monte Carlo Independent Column Approximation (McICA): Up and running in North America and Europe, Talk presented at the 17th Atmospheric Radiation Measurement (ARM) Science Team Meeting, Monterey, CA, March 26-30, 2007.
- Berg, R., National Hurricane Center Tropical Cyclone Report: Hurricane Joaquin (AL112015), National Hurricane Center, 36 pp., 2016.
- Bernardet, L., V. Tallapragada, S. Bao, S. Trahan, Y. Kwon, Q. Liu, M. Tong, M. Biswas, T. Brown, D. Stark, L. Carson, R. Yablonsky, E. Uhlhorn, S. Gopalakrishnan, X. Zhang, T. Marchok, B. Kuo, and R. Gall, Community Support and Transition of Research to Operations for the Hurricane Weather Research and Forecasting Model. *Bull. Amer. Meteor. Soc.*, 96, 953–960, 2015.
- Beven, J.L., R. Berg, and A. Hagen, National Hurricane Center Tropical Cyclone Report: Hurricane Michael (AL142018), National Hurricane Center, 86 pp., 2019.
- Biswas, M.K., and co-authors, Hurricane Weather Research and Forecasting (HWRF) Model: 2018 Scientific Documentation, National Center for Atmospheric Research, Developmental Testbed Center, 103 pp, 2018.
- Geleyn, J.F., Hollingsworth. A., An economical, analytical method for the computation of the interaction between scattering and line absorption of radiation, *Contrib. Atmos. Phys.*, 52, 1–16, 1979.
- Hogan, R.J., and A. Bozzo, ECRAD: A new radiation scheme for the IFS, Technical Memorandum 787, European Centre for Medium-Range Weather Forecasts, 33 pp., 2016.
- Hogan, R.J., Illingworth, A.J., Deriving cloud overlap statistics from radar. *Q. J. R. Meteorol. Soc.*, 126, 2903–2909, 2000.
- Iacono, M.J., and J.M. Henderson, Testing variations of exponential-random cloud overlap with RRTMG in HWRF, Project Final Report, Developmental Testbed Center, February, 2019. (Available at https://dtcenter.org/sites/default/files/visitor-projects/Iacono_Henderson_DTC_VP_FinalReport_2017-2018_0.pdf).
- Iacono, M.J., J.S. Delamere, E.J. Mlawer, M.W. Shephard, S.A. Clough, and W.D. Collins, Radiative forcing by long-lived greenhouse gases: calculations with the AER radiative transfer models, *J. Geophys. Res.*, 113, D13103, doi:10.1029/2008JD009944, 2008.
- Marciano, C.G. and G. M. Lackmann, The South Carolina flood of October 2015: Moisture transport analysis and the role of hurricane Joaquin, *J. Hydromet.*, 18, 2973–2990, doi:10.1175/JHM-D-16-0235.1, 2017.
- Miller, W. and D.-L. Zhang, Understanding the unusual looping track of Hurricane Joaquin (2015) and its forecast errors, *Mon. Wea. Rev.*, 147, 2231-2259, doi: 10.1175/MWR-D-18-0331.1, 2019.
- Nam, C., S. Bony, J.-L. Dufresne, and H. Chepfer, The ‘too few, too bright’ tropical low-cloud problem in CMIP5 models, *Geophys. Res. Lett.*, 39, L21801, doi:10.1029/2012GL053421, 2012.

- Oreopoulos, L., D. Lee, Y.C. Sud, and M.J. Suarez, Radiative impacts of cloud heterogeneity and overlap in an atmospheric General Circulation Model, *Atmos. Chem. Phys.*, 12, 9097-9111, 2012.
- Papin, P.P, R. D. Torn: An Analysis of Multiple Steering Influences on Tropical Cyclone Joaquin (2015), 32nd Conference on Conference on Hurricanes and Tropical Meteorology, San Juan, Puerto Rico, April 2016.
- Pincus, R., C. Hannay, S. A. Klein, K.-M. Xu, and R. Hemler, Overlap assumptions for assumed probability distribution function cloud schemes in large-scale models, *J. Geophys. Res.*, 110, D15S09, doi:10.1029/2004JD005100, 2005.
- Pincus, R., H. W. Barker, J.-J. Morcrette, A fast, flexible, approximate technique for computing radiative transfer in inhomogeneous cloud fields, *J. Geophys. Res.*, 108, D13, 2003.
- Shonk, J.K.P., R.J. Hogan, J.M. Edwards, and G.G. Mace, Effect of improving representation of horizontal and vertical cloud structure on the Earth's global radiation budget. Part I: Review and parametrization, *Q. J. R. Meteorol. Soc.*, 136, 1191–1204, 2010a.
- Shonk, J.K.P., and R.J. Hogan, Effect of improving representation of horizontal and vertical cloud structure on the Earth's global radiation budget. Part II: The global effects, *Q. J. R. Meteorol. Soc.*, 136, 1205–1215, 2010b.
- Wu, X., and X.-Z. Liang, Radiative effects of cloud horizontal inhomogeneity and vertical overlap identified from a month-long cloud resolving simulation, *J. Atmos. Sci.*, 62, 4105–4112, 2005.